

1 **Changes in excitability and ion channel expression in neurons of the major**
2 **pelvic ganglion in female type II diabetic mice**

3
4
5 Michael Gray^{1*}, Kawasi M. Lett^{1*}, Virginia B. Garcia¹, Cindy W. Kyi¹, Kathleen A. Pennington², Laura
6 C. Schulz², David J. Schulz¹

7
8 ¹ *Division of Biological Sciences, University of Missouri, Columbia, MO USA 65211*

9 ² *Department of Obstetrics, Gynecology and Women's Health, University of Missouri, Columbia, MO,*
10 *65211, USA.*

11 * *Denotes equal contribution by these authors*

12
13
14
15 **Abbreviated Title**

16 Changes in parasympathetic neurons in Type II diabetes

17
18 **Corresponding Author**

19 David J. Schulz, Ph.D.
20 Division of Biological Sciences
21 University of Missouri-Columbia
22 218 LeFevre Hall
23 Columbia, MO 65211
24 Ph 573-882-4067
25 Fax 573-884-5020
26 Email: schulzd@missouri.edu

27
28
29 **Acknowledgments**

30 This work was funded by a grant from the Missouri Spinal Cord Injuries Research Program (D.J.S.), the
31 Craig H. Neilsen Foundation (D.J.S.), American Diabetes Association Grant 1-14-BS-181 (L.C.S.) and
32 American Heart Association Postdoctoral Fellowship 13POST16910108 (K.A.P.). The authors declare no
33 competing financial interests.

34 **ABSTRACT**

35 Bladder cystopathy is a common urological complication of diabetes, and has been associated
36 with changes in parasympathetic ganglionic transmission and some measures of neuronal excitability in
37 male mice. To determine whether type II diabetes also impacts excitability of parasympathetic ganglionic
38 neurons in females, we investigated neuronal excitability and firing properties, as well as underlying ion
39 channel expression, in major pelvic ganglion (MPG) neurons in control, 10-week, and 21-week db/db
40 mice. Type II diabetes in *Lepr^{db/db}* animals caused a non-linear change in excitability and firing properties
41 of MPG neurons. At 10 weeks, cells exhibited increased excitability as demonstrated by an increased
42 likelihood of firing multiple spikes upon depolarization, decreased rebound spike latency, and overall
43 narrower action potential half-widths as a result of increased depolarization and repolarization slopes.
44 Conversely, at 21 weeks MPG neurons of db/db mice reversed these changes, with spiking patterns and
45 action-potential properties largely returning to control levels. These changes are associated with
46 numerous time-specific changes in calcium, sodium, and potassium channel subunit mRNA levels.
47 However, Principal Components Analysis of channel expression patterns revealed that the rectification of
48 excitability is not simply a return to control levels, but rather a distinct ion channel expression profile in
49 21-week db/db neurons. These data indicate that type II diabetes can impact the excitability of post-
50 ganglionic, parasympathetic bladder-innervating neurons of female mice, and suggest that the non-linear
51 progression of these properties with diabetes may be the result of compensatory changes in channel
52 expression that act to rectify disrupted firing patterns of db/db MPG neurons.

53

54 **Keywords: type II diabetes, diabetic cystopathy, autonomic ganglia, parasympathetic neurons,**
55 **excitability, electrophysiology**

56

57

58 INTRODUCTION

59 Diabetes is a systemic, progressive disease characterized by lack of insulin directly (Type I), or
60 functional lack of its effectors and/or insulin resistance (Type II), that ultimately leads to hyperglycemia
61 and chronic complications. Diabetes is the seventh leading cause of death in the United States and afflicts
62 11.1-11.9% of adults over the age of 20; this rate has increased from 8.9% in years 1988-1994 to 11.9 %
63 in years 2011-2014 (United States. Department of Health and Human Services. et al. 2016). In addition,
64 diabetic complications are age dependent (Gunnarsson 1975; DCCT Research Group 1996; Liu et al.
65 2017). This age dependence combined with the 111.5% increase in persons age 65 and older from 1975-
66 2015 (United States. Department of Health and Human Services. et al. 2016), necessitates studying an
67 important complication of diabetes—diabetic neuropathy.

68 Diabetic neuropathy is particularly dangerous due to its insidious development, susceptibility of
69 autonomic neurons and their subsequent regulation of vital organ systems, and a potential for positive
70 feedback loops through dysregulation of microvasculature (Faerman et al. 1971; Vinik et al. 2003).
71 Interventions are difficult as symptoms are subclinical and are often undiagnosed until long after neural
72 lesions occur. That is, autonomic motor neuron damage occurs long before patients report somatic
73 sensory symptoms. This is supported by the finding that in diabetic mice, thin, non-myelinated post
74 ganglionic autonomic motor neurons show deficits long before somatic sensory motoneurons do (Liu et
75 al. 2017). Neuropathic lesions can affect various autonomic pathways resulting in gastroparesis (Vinik et
76 al. 2003), cardiovascular dysregulation (Vinik et al. 2003, 2011), sudomotor dysfunction (Liu et al. 2017),
77 diabetic cystopathy (Faerman et al. 1971; Frimodt-Moller 1980; Kaplan et al. 1995; Vinik et al. 2003),
78 and dysregulation of blood flow in the periphery (UKPDS 1998). Bladder dysfunction as a result of
79 diabetes (i.e. diabetic cystopathy) is characterized by reduced bladder sensation, increased post-residual
80 void volume and overactive bladder (Kaplan et al. 1995; Yuan et al. 2015), and was first formally
81 described in diabetics in 1864 (Faerman et al. 1971). Some of the effects of diabetic cystopathy can be
82 attributed to damaged bladder afferents. For example, it has been shown in streptozocin (STZ) treated rats

83 (type I diabetes model) that diabetic cystopathy is correlated with reduced levels of nerve growth factor
84 (NGF) in dorsal root ganglion neurons (Sasaki et al. 2002). Furthermore, when NGF is expressed at the
85 bladder wall, the development of diabetic cystopathy and subsequent increased post residual void volume
86 can be mitigated (Sasaki et al. 2004). However, little is known as to how diabetes impacts autonomic
87 neurons innervating the bladder, and how this contributes to autonomic neuropathy and bladder
88 cystopathy.

89 The major pelvic ganglion (MPG) of the mouse is the primary motor innervation of the urinary
90 bladder. When examining motor neurons of this network in males, Tompkins et al. (2013), found that in
91 post-ganglionic, parasympathetic, MPG neurons in *Lepr^{db/db}* mice had an enhanced number of excitatory
92 post-synaptic potentials (EPSP) up to 20 seconds after pelvic nerve stimulation relative to control.
93 Simultaneously, the authors observed no change in EPSP amplitude. However, STZ-treated mice did not
94 differ in EPSP number and had significantly reduced amplitudes relative to control mice. This suggests
95 that the type I and type II models are distinct in how they affect physiology of MPG neurons.
96 Furthermore, change in action potential properties is similarly dependent on diabetic type: after-
97 hyperpolarization (AHP) duration was significantly decreased in *Lepr^{db/db}* mice, while being significantly
98 increased in STZ mice (Tompkins et al. 2013). Finally, MPG neuron input resistance and resting
99 membrane potential are decreased and depolarized, respectively, in *Lepr^{db/db}* mice but unaffected in STZ
100 mice (Tompkins et al. 2013). These results suggest that both EPSP and intrinsic properties of MPG
101 neurons are differentially modulated by the nature of the diabetic model.

102 In this study, we exploit the *Lepr^{db/db}* C57BL/6J mouse, to extend our understanding of how type
103 II diabetes affects progression of changes in neuronal excitability in neurons of the MPG of female mice.
104 Specifically, we examine how these conditions change neurons at 10- and 21-week time points by
105 combining current clamp recordings of neuronal output with ion channel expression analyses in the
106 MPGs of female mice. We predicted that firing properties and intrinsic properties should resemble that
107 observed by Tompkins et al. (2013); with a general increase in excitability at week 21 to evoked firing

108 rate, an increased RMP, decreased input resistance, and increased AHP duration. However, we observed a
109 distinct effect: excitability of MPG neurons was initially increased at 10-weeks, but subsequently became
110 less excitable again – towards baseline levels – at 21-weeks. These results suggest a compensatory change
111 in MPG neurons in diabetic animals. We then went on to investigate potential underlying mechanisms for
112 these changes via measurements of ion channel mRNA levels in MPGs from 10-week and 21-week
113 diabetic females.

114

115 **METHODS**

116 *Type II Diabetes Model – Lepr^{db/db} Animals*

117 Wild type (WT) C57BL/6J and Lepr^{db/db} female mice (*Mus musculus*) were obtained from the
118 Jackson Laboratory (Bar Harbor, ME, USA). Lepr^{db/db} mice have a mutation that interrupts the longest
119 isoform of the leptin receptor (Chen et al. 1996). These animals display hyperphagia, obesity,
120 hyperglycemia and hyperinsulinemia, which has led to their widespread use as a model of type II
121 diabetes. Together, mouse and rat leptin mutants have been used in over 4000 published studies of type II
122 diabetes (Wang et al. 2014). Lepr^{db/db} mice have been used by the Animal Models of Diabetic
123 Complications Consortium and others as models for diabetic neuropathy (Sullivan et al. 2007).

124 Mice were group housed in cages on a 12 hr. light/dark cycle and fed a standard chow diet ad
125 libitum. All animal procedures were performed in accordance with National Institutes of Health Guide for
126 the Care and Use of Laboratory Animals and approved by the University of Missouri Animal Care and
127 Use Committee.

128

129 *Establishing a Diabetic Phenotype*

130 *Glucose Measurement.* At either 10 (n = 15 WT and 14 $Lepr^{db/db}$) or 21 (n = 6 WT and 14
131 $Lepr^{db/db}$) weeks of age animals were fasted for 4 hours and then a fasting glucose measurement was taken
132 via tail blood using the average of two readings of a OneTouch® (Sunnyvale, CA) or ReliOn Prime®
133 (Arkay inc., Kyoto, Japan; Distributed by Walmart, Bentonville, AR) Blood Glucose Monitoring System.
134 At this time blood was collected to measure fasting serum insulin levels. Weights were also recorded at
135 this time.

136 *Insulin Elisa.* Serum insulin levels were analyzed using a Mouse/Rat Insulin Elisa (Millipore™,
137 Billerica, MA) according to manufacturer's instructions. A total number of 6 samples at 10 weeks were
138 run for both WT and $Lepr^{db/db}$ females. At 21 weeks of age 9 $Lepr^{db/db}$ and 6 WT females were analyzed.
139 For $Lepr^{db/db}$ serum was diluted at 1:20 with matrix solution provided in the ELSIA kit to allow for
140 measurements to fall on the standard curve.

141

142 *Electrophysiology*

143 MPGs were dissected from isoflurane euthanized female mice from wildtypes (n = 9) at 10 weeks
144 (WT), $Lepr^{db/db}$ at 10 weeks (n = 5; DB10), or $Lepr^{db/db}$ at 21 weeks (n = 5; DB21). Dissection and all
145 experiments were done in oxygenated physiological saline at room temperature. MPGs were dissected out
146 and pinned to a Sylgard (Dow, Midland, MI) lined perfusion chamber. The preparation was then
147 desheathed using small pins to remove excess tissue. Saline was composed of in mM: NaCl, 146; KCl,
148 4.7; $MgSO_4$, 0.6; $NaHCO_3$, 1.6; NaH_2PO_4 , 0.13; $CaCl_2$, 2.5; Glucose, 7.8; HEPES, 20; pH'd to 7.3.
149 Electrodes were pulled on a P-97 microelectrode puller (Sutter, Novato, CA) filled with 3M KCl, and had
150 resistances of 30 to 60 MΩ. Recordings were acquired in Bridge mode using an Axoclamp 900A and
151 digitized using a Digidata 1440A using the pClamp 10.3 suite of software (Molecular Devices,
152 Sunnyvale, Ca) running on an IBM-compatible computer. Silver electrode and ground wire were
153 chlorided using household Bleach (Clorox, Oakland, CA).

154

155 *Passive properties.* Resistance, time constant, capacitance and rebound spikes were estimated
156 from -500 pA current injections of 400 ms. In some protocols where there were no rebound spikes, these
157 properties were estimated from -500 pA current injections for 2000 ms, To ensure these protocols did not
158 differ, we examined action potential properties for 12 WT neurons where both protocols were used. A
159 paired t-test showed that hyperpolarization duration did not significantly affect these measurements, the
160 closest measurement to being affected was AHP ($t(11) = 2.090$, $p = 0.061$) while all other properties were
161 unaffected ($p > 0.1$). Due to the contamination of slow activating currents and membranes being non-
162 isopotential in real neurons, time was estimated by the 2 exponential fit; $V_m(t) = V_{final} + A_1 e^{-t/\tau_1} +$
163 $A_2 e^{-t/\tau_2}$; the larger A (IR) and time constant term were taken to be the time constant (Golowasch et al.
164 2009; White and Hooper 2013). Capacitance was estimated from this time constant and input resistance.
165 For excitability data, current was injected from 0 to 700 pA in 50 pA steps for 400 ms.

166 *Action Potential Properties.* Action potential properties were estimated both manually (Spike
167 count, Rheobase, AP slope to depolarizing current injection, and Threshold) and by using the auto-
168 statistics package of the Clampfit program from the pClamp 10.3 suite of software (Molecular Devices,
169 Sunnyvale, Ca) (All others). These properties are illustrated in figure 1 for reference, and unless otherwise
170 stated were performed on rebound spikes to prevent contamination from current injection.

171 *Threshold measurement.* Threshold was measured from two methods and verified by estimation
172 from passive properties and rheobase. First, we extrapolated manually from step protocols. Second, we
173 adopted an adapted version of the spike slope method, where the derivative of voltage with respect to time
174 slope is plotted vs voltage and the voltage at which this slope meets or exceeds some slope is threshold
175 usually set from 2 to 20 mV/ms (Naundorf et al. 2006; Platkiewicz and Brette 2010, 2011). However,
176 rather than using constant ascending spike slope, this method was adapted by measuring maximal
177 ascending slope within a 0.5 ms bin, defining threshold as the voltage recorded 0.25 ms before the center
178 point of the half maximal bin. Within wildtype, no significant differences were found between this

179 method ($M = -23.5$, $SD = 8.1$) and manual estimation ($M = -23.5$, $SD = 8.1$). Slope method was chosen to
180 minimize any confounds between changes in ascending slope.

181 *Inclusion Criterion.* Some neurons impaled produced no spikes. As we could not ascertain
182 whether this was due to impalement damage, or these cells being silent neurons or closely apposed
183 satellite glial cells (Hanani 2010), the following inclusion criteria were made: 1) All neurons must
184 produce spikes to depolarizing current injections. 2) All cells must have resting membrane potentials less
185 than -30 mV. 3) All cells must have input resistances greater than ~ 18 M Ω .

186 *Statistics.* Data was organized and stored in Microsoft Excel (Microsoft, Redmond, WA). All
187 Statistics and graphs were made in Sigmaplot 11.0 (Chicago, IL), R (<https://www.r-project.org/>) and
188 formatted in Adobe Illustrator CC 2017 (San Jose, CA). Data that passed normality testing and were
189 shown to be homoscedastic were analyzed using one-way ANOVA. Most Data, however, was found to be
190 non-normal and /or fail equal variance and comparisons were therefore made with a non-parametric
191 Kruskal-Wallis one-way ANOVA on ranks using a post-hoc Dunn's test. The two-way ANOVA for
192 Figure 3B failed the assumptions of normality and homoscedasticity and could not be successfully
193 transformed, statistics are reported for raw data.

194

195 *qRT-PCR Methods*

196 Paired MPGs from each animal were collected into Trizol reagent (Life Technologies, Carlsbad,
197 CA), homogenized, and stored at -80°C until RNA extraction. Total RNA was isolated from MPGs
198 according to the protocol provided by the manufacturer. Complementary DNA (cDNA) was generated
199 from 100 ng total RNA primed by a mixture of random hexamers and oligo-dT primers. Reverse
200 transcription reactions were carried out at a volume of 20 μl using qScript cDNA SuperMix (QuantaBio,
201 Beverly, MA) according to manufacturer protocols. Following cDNA synthesis, the reaction was heat
202 inactivated and diluted 5X to a final volume of 100 μl before being used as a template for quantitative

203 PCR (qPCR). From each cDNA reaction we quantified at least 15 different gene products. Multiple
204 cDNA synthesis reactions were carried out from a single total RNA sample to quantify the full suite of
205 genes examined in this study.

206 In our previous work, we designed or modified and independently validated qPCR primers for
207 use in absolute quantitation of mRNA copy number for all of the genes of interest in this study. These
208 primer sets are previously published, and standard curves generated and used as described in our previous
209 work (Garcia et al. 2014, 2018). Briefly, qPCR reactions were carried out using SYBR mastermix
210 (BioRad) according to the manufacturer's instructions, and consisted of primers at final concentrations of
211 2.5 μ M. Reactions were carried out on a CFXConnect (BioRad) machine with a three-step cycle of 95°C-
212 15s, 58°C-20s, 72°C-20s, followed by a melt curve from 65°C to 95°C. Fluorescence data acquisition was
213 made at the 72°C step, and every 0.5°C of the melt curve. All reactions were run in triplicate, and the
214 average Ct (cycle threshold) was used for interpolation with standard curves to generate copy number for
215 a given reaction.

216 The unit we use to express all of the qPCR data in this study is “copy number per ng of total
217 RNA,” and reflects the amount of input RNA that went into the cDNA synthesis reaction. All of the data
218 were normalized (see Garcia et al. 2014) relative to the average expression of Glyceraldehyde 3-
219 phosphate dehydrogenase (GAPDH), beta-actin, and hypoxanthine guanine phosphoribosyl transferase
220 (HPRT) genes from each sample (Vandesompele et al. 2002). Samples that were found to have low
221 expression of these control genes were eliminated from the analysis. None of the control genes showed
222 significant differences in expression across groups.

223

224 **RESULTS**

225 *Lep^{r^{db/db}}* mice produce a diabetic phenotype with hyperglycemia that differs according to age. Diabetic
226 neuropathy and the metabolic derangements of diabetes itself (Gunnarsson 1975; Giachetti 1978; Medici

227 et al. 1999) are age-dependent. Therefore, we wanted to verify that our $Lepr^{db/db}$ model exhibited diabetic
228 physiological properties such as weight gain, elevated blood sugar and serum insulin to verify our diabetic
229 model had sufficient time to develop the phenotype.

230 *Lepr^{db/db} mice are heavier than WT.* Mean weights (Figure 2A) for diabetic mice from weeks 10 to 21,
231 increased from 44.1 g (SD = 3.4) to 55.4 g (SD = 5.5), respectively (Holm-Šídák, $p < 0.001$) and were
232 significantly heavier than WT at both time points (Holm-Šídák, $p < 0.001$). In contrast, there was not a
233 statistically significant difference in weight for WT mice from week 10 (M = 18.9, SD = 1.6, g) to 21 (M
234 = 20.0, SD = 1.2, g) (Figure 2A, Holm-Šídák, $p = 0.082$). [Two way ANOVA: Genotype; $F(1, 43) =$
235 169.319 , $p < 10^{-8}$. Age; $F(1, 43) = 21.285$, $p = 3.5 \times 10^{-5}$. Interaction; $F(1, 43) = 3.401$, $p = 0.072$].

236 *Lepr^{db/db} mice are hyperglycemic, especially when young.* Surprisingly, in diabetic mice, fasting blood
237 glucose (Figure 2B) significantly *decreased* from 352.54 mg/dl (SD = 115.22) at week 10 to 196.62 mg/dl
238 (SD = 113.16) at week 21, this phenomena has been reported for C57BL/6J mice before, however,
239 usually at later time points (~week 25-30; although still elevated compared to control (Gunnarsson 1975).
240 Despite this, consistent with the diabetic phenotype, fasting blood glucose was significantly elevated in
241 diabetic mice for both week 10 (Holm-Šídák, $p < 0.001$) and week 21 (HS, $p = 0.044$) vs WT (Figure 2B).
242 In contrast to diabetic mice, no significant difference was observed in the fasting blood glucose of WT
243 mice between weeks 10 (mg/dl, M = 112.47, SD = 27.14) and 21 (M = 107.17, SD = 8.72; Holm-Šídák, p
244 = 0.901). [2-way ANOVA: Genotype; $F(1, 43) = 37.150$, $p = 2.7 \times 10^{-7}$. Age; $F(1, 43) = 8.893$, $p =$
245 0.005. Interaction; $F(1, 43) = 7.762$, $p = 0.008$].

246 *Lepr^{db/db} mice have elevated plasma insulin.* In C57BL/6J $Lepr^{db/db}$ mice the plasma insulin level is known
247 to increase (Gunnarsson 1975). Mean plasma insulin levels (Figure 2C) in diabetic mice were stable from
248 week 10 (ng/ml, M = 29.51, SD = 40.19) to week 21 (ng/ml, M = 35.11, SD = 46.51; Holm-Šídák, $p =$
249 0.908), but were significantly elevated compared to WT (Holm-Šídák, $p < 0.001$) which also did not
250 change from weeks 10 (ng/ml, M = 0.51, SD = 0.43) to 21 (ng/ml, M = 0.33, SD = 0.07; Holm-Šídák, $p =$

251 0.817). Together, these results support that the $Lepr^{db/db}$ manifests the insulin resistant, type II diabetic
252 phenotype.

253

254 *Firing properties of $Lepr^{db/db}$ neurons changes with diabetic condition and time*

255 *DB10 and DB21 neurons have enhanced and reduced excitability, respectively.* Our hypothesis
256 was that since diabetes causes diabetic cystopathy (Kebapci et al. 2007), presumably at least in part
257 through diabetic autonomic dysregulation (Nadelhaft and Vera 1992), $Lepr^{db/db}$ efferent bladder-
258 innervating neurons of the MPG may contribute to these pathological changes and may manifest
259 themselves as changes in intrinsic excitability. Therefore, we first examined whether MPG neurons from
260 different diabetic conditions would spike differently in response to depolarizing current steps from 0 to
261 +700 pA in 50 pA increments (Figure 3A). We used 114 cells from 10-week-old WT mice (WT, n = 37);
262 5, 10-week-old diabetic mice (DB10, n = 41) and 5, 21-week-old diabetic mice (DB21, n = 36). As we
263 saw no difference in metabolic parameters for WT mice from weeks 10 to 21 (Figure 2), we assume WT
264 physiology is likewise similar to WT21. Thus all WT recordings are made from 10-week old animals. The
265 representative neurons in Figure 3A show that DB10 (Red) neurons appear to be more excitable than WT
266 (Black). In contrast, DB21 neurons (Green) were less excitable than either DB10 or DB21, and appeared
267 to have reduced input resistance (discussed below). Surprisingly, across all conditions, of the 114 neurons
268 studied, only 13 (11.4%) produced more than one spike at any current injection level. Of the neurons that
269 spiked more than once, 76.9% (10/13) were in the DB10 condition compared to a 15.4% (2/13) and 7.7%
270 (1/13) contribution from WT and DB21 groups respectively. The probability of finding a neuron spiking
271 more than once was 5.4% (2/37), 24.4% (10/41) and 2.8% (1/36) for WT, DB10 and DB21 groups
272 respectively. Supporting this difference in excitability, a Chi square test showed that these groups were
273 not statistically independent (χ^2 (2, N = 114) = 8.268, p = 0.016). Similarly; a Kruskal-Wallis showed this
274 data was significantly different, however, this test is more dubious as all groups had median = 1 (Table 1).
275 Due to this low spike probability, we could not run more conventional IO curves. Therefore, instead of IO

276 curves, we examined the cumulative probability of producing one or more spikes as a function of current
277 injected. A two way ANOVA for factors current and condition showed that cumulative probability of
278 firing 1 or more spikes as a function of injected current was reduced in DB21 condition [Condition; $F(2,$
279 $1443) = 37.997$, $p < 1 \times 10^{-8}$. Current; $F(12, 1443) = 51.817$, $p < 1 \times 10^{-8}$. Interaction; $F(24, 1443) =$
280 2.038 , $p = 0.002$.]. The probability of a neuron firing at least once (Top, Figure 3C) was not significantly
281 different between DB10 and WT neurons (Holm-Šídák, $p = 0.883$), in contrast, DB21 had reduced
282 probability of firing at least one spike from current injections of 100 to 350 pA when compared to DB10
283 (Holm-Šídák $p < 0.05$) and from 100 to 400 pA when compared to WT (Holm-Šídák $p < 0.05$).
284 Unfortunately, this particular distribution was neither normally distributed nor homoscedastic due to its
285 binary nature. Supporting the reduced excitability of DB21 neurons was the finding that median rheobase
286 (Left, Figure 3B) was increased in DB21 (Mdn = 300 pA, IQR = 450-200, pA) relative to WT (Mdn =
287 175, IQR = 262.5-100, pA) (Dunn's test, $p < 0.01$) and DB10 (Mdn = 150, IQR = 250-100, pA) (Dunn's
288 test, $p < 0.01$) [Kruskal Wallis ANOVA on Ranks; $H(2) = 16.181$, $p < 0.001$]. Together, these data
289 support DB21 mice having reduced MPG excitability.

290

291 *DB10 condition enhances excitability.* When examining the probability of these neurons firing twice or
292 more, neurons from DB10 had significantly greater probability of firing more than two spikes compared
293 to both WT and DB21 (Bottom, Figure 3C). This change was significant from current ranges 350-700 pA
294 vs DB21 (Holm-Šídák, $p < 0.05$) and 400-700 pA vs WT (Holm-Šídák, $p < 0.05$) [Condition; $F(2, 1443)$
295 $= 43.428$, $p < 1 \times 10^{-8}$. Current; $F(12, 1443) = 2.251$, $p = 0.008$. Interaction; $F(24, 1443) = 1.301$, $p =$
296 0.150 .]. Median DB10 rheobase (Left, Figure 3B; Mdn 150, IQR = 250-100, pA) was not significantly
297 different from WT (Mdn 150, IQR = 275-100, pA) (Dunn's, $p > 0.05$), but was significantly less
298 compared to DB21 (Mdn 300, IQR = 450-200, pA) (Dunn's, $p < 0.05$) [Kruskal-Wallis, $H(2) = 16.053$, p
299 < 0.001]. In agreement with this, DB10 threshold (Center, Figure 3B; Mdn = -25.0, IQR = -20.5-(-30),
300 mV) was hyperpolarized compared to DB21 (Mdn = -19.5, IQR = -15-(-24), mV) (Dunn's test, $p < 0.01$),

301 however, it was not significantly different from WT (Mdn = -22.0, IQR = -18-(-27.5), mV) but [Kruskal
302 Wallis ANOVA on Ranks; $H(2) = 9.351$, $p = 0.009$]. These results, suggest that DB10 excitability is
303 enhanced relative to WT and DB21 conditions.

304

305 *Rebound spike latency is decreased in DB10 neurons.* Another sign that excitability was increased in
306 DB10 neurons was that latency to first spike after release of hyperpolarizing current injection (Right,
307 Figure 3B) was significantly decreased in the DB10 condition (; Mdn = 7.9, IQR = 13.9-7.1, ms)
308 compared to WT (Mdn = 15.4, IQR = 20.9-11.5, ms)(HS, $p < 0.05$) and DB21 (Mdn = 15.7, IQR = 21.2-
309 14.1, ms) (Holm-Šídák, $p < 0.05$) conditions. These data support excitability being enhanced in the DB10
310 condition.

311

312 *Passive properties of diabetic neurons change with age and diabetic condition*

313 In order to characterize the mechanism of observed changes in firing of MPG neurons, we first
314 examined passive properties with the prediction that we should observe depolarized resting membrane
315 potential (RMP) and reduced input resistance in diabetic neurons . In contrast to Tompkins et al. (2013),
316 our data showed no difference in median resting membrane potential (Figure 4A) between WT (Mdn = -
317 43.0, IQR = -36.5-(-47.0), mV) , DB10 (Mdn = -42.0, IQR = -39.5-(-48.5), mV) or DB21 (Mdn = -40.0,
318 IQR = -38.0-(-45.5), mV) (Figure 4A) [Kruskal-Wallis ANOVA on ranks; $H(2) = 2.018$, $p = 0.365$].
319 However, consistent with Tompkins et al. and our finding of rheobase being increased in DB21, we found
320 that median input resistance (Figure 4B) was significantly reduced in DB21 (Mdn = 42.5, IQR = 51.8-
321 37.3, M Ω) (Dunn's test; $p < 0.004$) but not in DB10 (Mdn = 51.0, IQR = 89.0-38.0, M Ω) (Dunn's test, p
322 > 0.05) neurons vs WT (Mdn = 68, IQR = 89.0-44.0, M Ω) neurons [Kruskal-Wallis ANOVA on ranks, H
323 $(2) = 10.641$, $p = 0.005$]. We next estimated time constant by a 2-exponential fit (Golowasch et al. 2009;
324 White and Hooper 2013). Median time constant (Figure 4C) showed a similar pattern, showing a

325 significant reduction in DB21 (Mdn = 1.8, IQR = 2.5-1.5, ms) compared to WT (Mdn = 2.3, IQR = 3.2-
326 1.6, ms) (Dunn's test, $p < 0.01$), but not compared to DB10 (Mdn = 2.5, IQR = 4.2-1.7, ms)(Dunn's test,
327 $p > 0.05$ [Kruskal-Wallis one way ANOVA on ranks, $H(2) = 6.805$, $p = 0.033$]. Capacitance (Figure 4D)
328 showed a different pattern, where both DB10 (Mdn = 48.7, IQR = 57.8-39.6, pF) and DB21 (Mdn = 41.9,
329 IQR = 54.8-35.1, pF) were significantly increased relative to WT (Mdn = 32.9, IQR = 40.2-29.8, pF)
330 (Dunn's test, $p < 0.01$) [[Kruskal-Wallis one way ANOVA on ranks, $H(2) = 23.187$, $p < 0.001$]. These
331 data suggest that capacitance is increased with diabetic condition independent of time, while time
332 constant and resistance change with diabetic condition and age.

333

334 *Action potential properties in diabetic neurons change with age.*

335 In order to establish how observed changes in excitability caused by diabetic condition occurred,
336 we examined whether diabetic condition and age modulated properties of the action potentials shown in
337 figure 1.

338 *Ascending spike slope is increased in response to depolarizing current injection in the DB10 condition*
339 *but not first rebound spike.* We looked at ascending action potential slope ($\frac{dv}{dt}$) in response to depolarizing
340 current injections (Figure 1, 9). DB10 mice had significantly greater median ascending spike slope
341 (Figure 5A, Mdn = 30.0, IQR = 52.5-9.5, mv/ms) compared to either WT (Mdn = 8, IQR = 19.0-3.3,
342 mv/ms) (Dunn's Test; $p < 0.01$) or DB21 mice (Mdn = 5, IQR = 20.3-3.0, mv/ms) (Dunn's Test; $p < 0.01$)
343 [Kruskal-Wallis ANOVA on Ranks; $H(2) = 22.365$, $p < 0.001$]. Interestingly, in contrast to evoked
344 spikes, when we examined median maximum ascending slope (i.e. bins of 0.02 ms; Figure 1, 10), in
345 rebound spikes, DB10 neurons (Figure 5C, Mdn = 62.8, IQR = 77.9-40.3, mv/ms) did not significantly
346 differ from WT (Mdn = 55.3, IQR = 77.9-40.3, mv/ms) or DB21 (Mdn = 40.3, IQR = 56.6-25.6,
347 mv/ms)[Kruskal-Wallis ANOVA on Ranks; $H(2) = 5.670$, $p = 0.059$]. We believe this difference was
348 real and not due to a reduction in statistical power, as within WT groups, the coefficient of variance in

349 ascending slope for depolarizing current injections was greater (CV = 1.14) than for rebound spikes (CV
350 = 0.79) . In support of there being no differences in rebound spikes, when ascending spike slope was
351 quantified using a 10-90% rise slope criterion (Figure 1, 7), DB10 neurons (Figure 5G, Mdn = 29.8, IQR
352 = 40.6-15.4, mv/ms) did not significantly differ from either WT (Mdn = 25.8, IQR = 39.5-12.4, mv/ms)
353 or DB21 (Mdn = 20.0, IQR = 32.7-11.5, mv/ms) [Kruskal-Wallis ANOVA on Ranks; $H(2) = 2.043$, $p =$
354 0.360]. These data support spike slope increasing in the DB10 condition in response to depolarization
355 driven spikes but not rebound spikes.

356 *AP half-width is decreased while decay slope is increased in rebound spikes of DB10 neurons.* In contrast
357 to ascending slope, we found that the median width of the action potential at half its maximal height (i.e.
358 half-width; Figure 1, 3) was significantly reduced in the DB10 condition (Figure 5B, Mdn = 3.0 IQR =
359 3.3-2.4, ms) compared to DB21 (Mdn = 3.7, IQR = 4.4-3.1, ms) (Dunn's test, $p < 0.01$) but not vs WT
360 (Mdn = 3.3, IQR = 4.4-2.6, ms) (Dunn's test, $p > 0.05$) [Kruskal-Wallis ANOVA on Ranks; $H(2) =$
361 14.991 , $p < 0.001$].

362 Part of the reduction in DB10 half-width may be explained by the finding that that both maximal
363 and 90-10% decay slope increased (Also see discussion). This is shown as median maximal decay slope
364 (Figure 5D) was made more negative (increased) in DB10 neurons (Mdn = -20.0, IQR = -14.7-(-24.6),
365 mv/ms) vs DB21 neurons (Mdn = -13.4, IQR = -9.7-(-18.9), mv/ms) (Dunn's test, $p < 0.05$) but not vs
366 WT (Mdn = -16.0, IQR = -11.3-(-22.1), mv/ms) (Dunn's test, $p > 0.05$) neurons [Kruskal-Wallis ANOVA
367 on Ranks; $H(2) = 8.112$, $p = 0.017$] suggesting these neurons repolarized faster. In agreement with this,
368 mean 90-10% decay slope (Figure 5H) also became more negative in the DB10 condition($M = -16.7$, SD
369 $= 5.3$, mv/ms) vs WT ($M = -12.4$, $SD = 5.6$, mv/ms) (Holm Sidak, $p = 0.001$) and compared to DB21($M =$
370 -11.0 , $SD = 4.2$, mv/ms), mv/ms)(Holm-Sidak, $p < 0.001$) [One way ANOVA; $F(2, 100) = 11.541$, $p =$
371 3.1×10^{-5}]. Accordingly, median 90-10% decay time (Figure 5F) significantly decreased in DB10 (Mdn =
372 2.7, IQR = 3.1-2.5, ms) vs WT (Mdn = 3.7, IQR = 4.8-3.0, ms) (Dunn's test, $p < 0.01$) and DB21 (Mdn =
373 4.4, IQR = 5.0-3.5, ms) (Dunn's test, $p < 0.01$) [Kruskal-Wallis ANOVA on Ranks; $H(2) = 42.223$, $p <$

374 0.001]. This data, in combination with the finding that AP ascending slope did not increase in rebound
375 spikes, suggests that AP half-width decreased primarily through a mechanism that increases AP
376 descending slope.

377 *AP area and AHP decay constant decreased in DB10 with no changes in after hyperpolarization*
378 *(AHP) area.* Consistent with decreased AP half-width, total AP area (excluding the AHP; Figure 5I) was
379 significantly decreased in DB10 neurons (Mdn = 174.4, IQR = 238.8-142.7, mV·ms) relative to DB21
380 (Mdn = 232.5, IQR = 266.7-217.5, mV·ms)(Dunn's test, $p < 0.05$) but not when compared to WT (Mdn =
381 209.8, IQR = 290.7-172.0, mV·ms) (Dunn's test, $p > 0.05$) [Kruskal-Wallis ANOVA on Ranks; $H(2) =$
382 12.320, $p = 0.002$]. This was not due to changes in spike height, as neither DB10 (Mdn = 63.6, IQR =
383 78.1-37.9, mV) nor DB21 (Mdn = 61.2, IQR = 75.9-53.8, mV) differed significantly in spike height
384 (Table 1) relative to WT (Mdn = 64.5, IQR = 80.1-52.7, mV) [Kruskal-Wallis ANOVA on Ranks; $H(2) =$
385 0.498, $p = 0.779$]. If AP area decreased, a possible mechanism would be activation of outward currents,
386 and one might expect to see an enhanced AHP. However, no change in AHP area (Figure 5J) for DB10
387 (Mdn = -141.6, IQR = -88.1-(-259.2), mV·ms), nor DB21 (Mdn = -121.9, IQR = -92.1-(-200.5), mV·ms)
388 vs WT (Mdn = 116.6, IQR = -80.6-(-251.1), mV·ms) was observed [$H(2) = 0.530$, $p = 0.767$]. Neither
389 were changes were observed in AHP height (figure 1, 2) in DB21 (Figure 5K, Mdn = -10.0, IQR = -5.8-(-
390 12.9), mv), DB10 (Mdn = -11.6, IQR = -7.7-(-15.4), mv) conditions vs WT (Mdn = -12.4, IQR = -8.5-(-
391 15.9), mv) [Kruskal-Wallis ANOVA on Ranks; $H(2) = 2.900$, $p = 0.235$]. Despite our finding of stable
392 AHP amplitude and area, we did see that AHP decay tau significantly decreased in DB10 neurons (Mdn =
393 13.0, IQR = 16.5-10.5, ms) vs WT (Mdn = 16.9, IQR = 21.2-16.9, ms) (Dunn's, $p < 0.01$) and DB21
394 (Mdn = 17.0, IQR = 20.0-13.4, ms) (Dunn's, $p < 0.05$) (Figure 5L) [Kruskal-Wallis ANOVA on ranks; H
395 $(2) = 11.896$, $p = 0.003$]. These data suggest that diabetic condition and age affect interact to alter AP
396 area and AHP decay constant while leaving other AP parameters unmodified.

397 *2nd AHPs and ADPs after 145 ms.* When quantifying properties of the AHP, it was found that
398 after the initial AHP, some neurons had after depolarizations, while some had secondary slower AHPs

399 and still others had both. We attempted to systematically quantify this across conditions by analyzing the
400 change in voltage 145 ms after the descending stroke of the AP recrossed baseline. However, this comes
401 with the caveat that some neurons could not be quantified due to no change in baseline, multiple rebound
402 spikes, or loss of cells. Within 73.0 % (27/37) of quantified WT neurons, 81.5% (22/27) displayed
403 afterdepolarizations, while the remaining 18.5% (5/27) displayed secondary after hyperpolarizations and
404 none displayed both. Within DB10 neurons 4.9% (2/41) could not be classified due to multiple rebound
405 spikes. However, of the 82.9% (34/41) that could be quantified, 44.1% (15/34) showed ADPs, 20.6%
406 (7/34) showed secondary AHPs; in contrast to WT; where 29.4% (10/34) of these neurons showed both
407 AHPs and ADPs. Within 94.4% (34/36) of quantified DB21 neurons, 76.5% (26/34) showed ADPs, 2.9%
408 (1/34) showed secondary AHPs, while 20.6% (7/34) showed both. A Chi Square test showed that these
409 groups were statistically independent (χ^2 (4, N = 95) = 15.960, $p = 0.003$). Alternatively, when we just
410 quantified the absolute voltage change at 145 ms, DB10 (Mdn = -0.2, IQR = 2.0-(-0.7), ΔmV) (Dunn's, p
411 < 0.05) but not DB21 (Mdn = 0.8, IQR = 1.8-0.9, ΔmV) (Dunn's, $p > 0.05$) was significantly different
412 from WT (Mdn = 1.8, IQR = 3.8-0.9, ΔmV) (Table 1) [Kruskal-Wallis ANOVA on Ranks; $H(2) =$
413 10.766, $p = 0.005$]. This data suggests that the DB10 condition is more likely to have slow AHPs or a lack
414 of ADPs relative to WT.

415

416 *Ion Channels Show Widespread Changes in Expression in Both DB10 and DB21 Animals*

417 We specifically focused on subsets of ion channel and receptor genes for this study to start to
418 understand the underlying mechanisms for changes in excitability that we detected in MPG neurons of
419 diabetic animals. We sampled alpha subunits for voltage-dependent Ca^{2+} channels (*CACNA1A-H*), a
420 subset of Na^+ channels (*SCNx*), and six families of K^+ channels (*KCNA*, *KCNB*, *KCNC*, *KCND*, *KCNN*,
421 *KCNMA*). Of 30 ion channel genes studied, 8 were significantly different between DB10 and control
422 wild-type animals (Figure 6). The voltage-dependent Ca^{2+} channels *CACNA1A*, *CACNA1E* and
423 *CACNA1H* were significantly higher in DB10 animals relative to control. The only Na^+ channel gene that

424 was changed was a significant increase in *SCN2A1* in DB10 animals. In addition, 4 K⁺ channel genes
425 showed altered expression in DB10 animals: *KCNA3* was significantly lower in DB10 animals, while
426 *KCNB1*, *KCNC2*, and *KCND3* were significantly higher in DB10 mice.

427 In DB21 animals, 12 channel genes showed differential expression relative to wild-type controls
428 (Figure 6). *CACNA1D* and *CACNA1G* were significantly higher in DB21 animals relative to control.
429 There were no significant differences in sodium channel gene expression seen between DB21 and wild-
430 type animals. However, there were 10 different K⁺ channel genes that showed changes in expression in
431 DB21 animals. *KCNA2*, *KCNA3*, *KCNA5*, and *KCNC3* all were significantly lower in DB21 animals than
432 wild-type, with *KCNA2* and *KCNC3* expression all but abolished in the DB21 animals. *KCNC4*, *KCND2*,
433 *KCND3*, *KCNN1*, *KCNN3* and *KCNMA1* were all significantly higher in DB21, with *KCND2* expression
434 only detectable in DB21 animals. Most of these changes are seen only in DB21 animals and not in DB10,
435 including *KCNA2*, *KCNA5*, *KCNC3*, *KCNC4*, *KCND2*, *KCNN1*, *KCNN3* and *KCNMA1*.

436 Some changes seen in DB10 animals resolve to control levels in the DB21 animals, while others
437 persist throughout the DB21 time point (Figure 6). *KCNA3* is significantly lower in DB10 animals, and
438 this change persists into the DB21 group. *KCND3* is significantly increased in both DB10 and DB21
439 animals. Conversely, *KCNB1* is significantly higher in the DB10 animals, but returns to control levels in
440 DB21 animals. Finally, there are some channels that are significantly different only between DB10 and
441 DB21. *KCNA1* and *KCND1* are significantly higher in DB21 than DB10, although there is a trend
442 towards these two channels being downregulated in DB10 overall, even though this does not reach
443 statistical significance relative to control. The converse is true for *KCNB2*, which is significantly higher in
444 DB10 than DB21 – although there is a trend for this channel to be transiently upregulated in the DB10
445 group.

446

447 *Principal Components Analysis to Further Examine Differences Among Groups in Firing Properties and*
448 *Channel Expression*

449 We next used principal component analysis (PCA) to visualize potential patterns and correlations
450 in the features that may underlie distinctions in both the spike properties and channel expression across
451 groups. A variance plot of the first two principal components (PC) for spike characteristics (Figure 7A)
452 demonstrates that there is overlapping features in all three groups that do not distinguish these groups in
453 any obvious way. There is one major PC (PC1) that accounts for the majority of the variance in the data
454 42.5%, Figure 7B). The variables that most contribute to the variance in spike characteristics largely
455 consist of features involved in shaping the action potential dynamics underlying spike shape, such as
456 decay slope, rise slope, and the amplitude of the spike (e.g. spike height, peak amplitude). These would
457 consistent with changes in Na⁺ and K⁺ channel expression, particularly those subtypes involved in the
458 spiking itself. However, there is no combination of features that separates the diabetic animals from the
459 wild-types, or each other, in a discrete fashion.

460 The PCA for channel expression in the MPG tells a different story. The variance plot of PC1 and
461 PC2 (Figure 8A) shows clear separation of all three groups, and the scree plot (Figure 8B) notes that these
462 two PCs account for the majority of the variance in the data. When looking at the channels that contribute
463 to PC1 and PC2, it is also clear validation of the changes in expression reported in Figure 6. By
464 examining the vector plot in Figure 8A and the contributions to PC1 in Figure 8B, it is possible to
465 discriminate a group of channels largely responsible for distinguishing the DB21 animals. The top ten
466 contributors to PC1 consists entirely of channels that are uniquely differentially expressed in DB21
467 animals relative to both DB10 and control. Conversely, by examining the top ten contributors to PC2 – in
468 conjunction with the vector plot – it can be seen that PC2 consists of channels uniquely differentially
469 expressed in DB10 animals (*CACNA1A*, *CACNA1E*, *SCN2A1*, *KCNB1*, *KCNC2*) as well as channels that
470 are both changed in the same direction in DB10 and DB21 (*KCND3*).

471

472 **DISCUSSION**

473 Diabetic cystopathy has formally been documented since 1864 (Faerman et al. 1971), yet the only direct
474 attempt to document how diabetes impacts efferent bladder innervating neurons was by Tompkins et al.,
475 (2013) who focused largely on synaptic properties. Therefore, in this study we attempted to identify for
476 the first time the impacts of a type II diabetes model on the intrinsic properties of bladder-innervating
477 parasympathetic neurons in female mice. We hypothesized that passive properties, overall excitability and
478 action potential properties in MPG neurons would change in an age-dependent manner within the diabetic
479 condition. Furthermore, we examined underlying changes in mRNA levels for voltage-dependent ion
480 channels in the whole ganglion as a reflection of the most salient of changes in excitability and firing of
481 MPG neurons.

482 $Lepr^{db/db}$ mice on the C57Bl6/J strain used here model hyperglycemia and persistent
483 hyperinsulinemia with beta cell hypertrophy, whereas those on the BKS background strain progress to
484 beta cell failure (Hummel et al. 1972). Although the mice in this study were diabetic at both ages, their
485 hyperglycemia was somewhat worse at 11 weeks than at 21 weeks, consistent with previous observations
486 in this strain (Breyer et al. 2005; Sullivan et al. 2007). This improvement was consistent with the
487 constant, or slightly increasing serum insulin concentrations at 21 weeks, indicating that while the beta
488 cells are not able to adequately compensate for insulin resistance, they have not undergone beta cell
489 failure.

490

491 *Diabetes interacts with time to first increase then decrease MPG neuron excitability*

492 One of our most important findings was that excitability of MPG neurons in $Lepr^{db/db}$ females changes
493 nonlinearly with the amount of time exposed to the diabetic environment. Specifically, we observed that
494 10 week $Lepr^{db/db}$ mice had an increased probability of firing two or more spikes, and decreased rebound
495 spike latency; both of which are measures of increased overall neuronal excitability. In contrast, week 21

496 $Lepr^{db/db}$ neurons changed in the opposite direction, exhibiting a decrease in spike probability and
497 increased rheobase, both of which are indications of lower overall excitability. This trend of a change in
498 firing properties at 10 weeks that is then rectified at 21 weeks is also seen in the characteristics of action
499 potentials of MPG neurons. Specifically, spikes are narrower (as seen by a decreased half-width,
500 increased ascending slope and enhanced decay slope, and decreased decay time in DB10 animals), and
501 AHPs are shorter are in the DB10 animals but return to control levels in the DB21 group. These data are
502 consistent with the hypothesis that long-term diabetes results in change in MPG neuron that potentially
503 are compensated for via long-term plasticity mechanisms in the DB21 animals. Regardless of whether the
504 changes in excitability and action potential properties are compensatory or represent disease progression
505 in the context of the entire LUT, there is clear change in the characteristics of MPG neurons over the
506 course of 10-21 weeks in diabetic animals.

507 Because normal bladder function and diabetic cystopathy are the result of a complex interaction
508 of the activities of sympathetic, parasympathetic, and sensory feedback mechanisms combined with
509 bladder compliance and detrusor properties, it is not possible to interpret our results directly in context of
510 mechanisms of changes in bladder output as a result of diabetes. However, the time course of changes in
511 MPG neuron excitability mirror those of bladder output over the progression of diabetic cystopathy in
512 rodents. For example, in type I diabetic mice there is a sharp decline in basal bladder pressure and mean
513 threshold pressure from weeks 9-12 that then is rectified to control levels by 20 weeks (Daneshgari et al.
514 2006a). Similar time course changes in bladder output features as measured by cystometrogram have been
515 documented in rats as well, whereby diabetic bladders transition from compensated to decompensated
516 states between 9-12 weeks following onset of diabetes (Daneshgari et al. 2006b). Therefore, while a direct
517 mechanistic link to bladder output cannot be made from our data, the results are consistent with the
518 overall change in LUT output over the time course of diabetic cystopathy.

519

520 *Potential mechanistic insights via interpretation of changes in mRNA levels*

521 It would be an over-interpretation to directly infer mechanisms underlying physiological changes
522 in single neurons from data collected at the mRNA level from whole ganglia. However, the steady-state
523 mRNA levels for ion channels provide a high-throughput opportunity to generate hypothesis regarding
524 underlying mechanistic changes in ionic currents. Indeed, we see multiple changes in channel mRNAs
525 that are consistent with the physiological changes we report. In this section, we will highlight some of the
526 most salient changes we found at the level of neuronal properties, and cautiously hypothesize on potential
527 underlying mechanism via changes at the mRNA level.

528 In 10-week *Lepr^{db/db}* mice we observed that although rheobase did not change, several properties
529 associated with excitability did change. The most salient of these properties was the increase of the
530 probability of firing 2 or more spikes. As shown in Figure 3A and also previously documented (Suzuki
531 and Rogawski 1989; Tompkins et al. 2013), MPG neurons can spike once or many times, a phenomena
532 observed in many other autonomic neuron types (Cassell et al. 1986; Malin and Nerbonne 2001; Springer
533 et al. 2015). One obvious possible mechanism for generating multiple spikes is the activation of a
534 depolarizing current with somewhat slower kinetics that can maintain depolarization above threshold to
535 allow for the generation of multiple spikes. Our data show changes in channel expression that are
536 consistent with this hypothesis. In particular, there is a significant increase in mRNA levels for the
537 calcium channels *CACNA1A*, *CACNA1E*, and *CACNA1H* in DB10 animals relative to both WT and
538 DB21. Furthermore, *CACNA1E* levels overall are the most abundant calcium channel mRNA that we
539 detected, with levels an order of magnitude higher than any other calcium channel subunit. *CACNA1E*
540 encodes the R-type current $Ca_v2.3$, which is known to make up ~25% of total calcium current in rat MPG
541 neurons (Won et al. 2006), and $Ca_v3.2$ – encoded by *CACNA1H* – is the predominant T-type channel in
542 rat MPG (Lee et al. 2002). R-type currents are known to influence bursting output in CA1 pyramidal
543 neurons (Metz et al. 2005), and T-type currents in many neurons trigger low-threshold spikes, which in
544 turn generate bursts of action potentials (Perez-Reyes 2003). While the interplay of multiple calcium
545 channel subunits and the remaining ionic conductances of the cell are quite complex in terms of

546 generating different output patterns, increases in R-type and T-type currents would be a feasible way to
547 influence the multiple spiking phenotype in DB10 animals.

548 We also observed increased ascending and descending spike slopes, and decreased spike half-
549 width in the DB10 animals relative to WT and DB21. We observed increased expression of mRNAs
550 coding for $\text{Na}_v1.2$ (*SCN2A1*), as well as a trend for increased $\text{Na}_v\beta1$ (*SCN1B*) expression, in the DB10
551 animals. $\text{Na}_v1.2$ channels are largely localized to the axons and initial segments of unmyelinated neurons
552 (Vacher et al. 2008), which is consistent with the post-ganglionic fibers of the MPG. $\text{Na}_v\beta1$ is known to
553 interact with $\text{Na}_v1.2$ channels to increase surface expression of these subunits (Isom et al. 1995).
554 Therefore, increases in expression of *SCN2A1* and *SCN1B* would be expected to increase AP upstroke,
555 which was observed for depolarizing current injections but not rebound spikes. In addition, $\text{K}_v3.2$ and
556 $\text{K}_v2.1$ are potassium channels with relatively high threshold activation and fast deactivation such that they
557 have both been implicated as large contributors to the AP repolarization and as a consequence decrease
558 AP width (Rudy and McBain 2001; Liu and Bean 2014). The upregulation of their constituent mRNA
559 subunits (*KCNC2* and *KCNB1* respectively) is entirely consistent with the firing phenotypes observed.

560 As we observed increases in ascending spike slope to depolarizing current injections, but not
561 rebound current injections in DB10 neurons, it is possible that high threshold potassium currents with fast
562 deactivation time constants could play a role in permitting multiple spikes during depolarizing current
563 injections by enhancing sodium channel de-inactivation. As K_v2 family members are known to encode
564 delayed rectifiers, and K_v3 channels have fast activation and deactivation rates associated with sustained
565 higher-frequency firing, then the fact that we see increased $\text{K}_v3.2$ (*KCNC2*) and $\text{K}_v2.1$ (*KCNB1*)
566 expression is also consistent with these results. While this is well documented for $\text{K}_v3.2$ as it is a high
567 threshold, fast deactivating (Weiser et al. 1994; Rudy and McBain 2001) ion channel, it is less clear that
568 this is the case for $\text{K}_v2.1$ as it is intermediate in these parameters. For example, in the superior cervical
569 ganglion (SCG) neurons, $\text{K}_v2.1$ has somewhat high $V_{1/2}$ activation, slow activation, slow or no
570 inactivation, but a relatively fast deactivation (Liu and Bean 2014). If $\text{K}_v2.1$ is playing a role in keeping

571 the functional pool of sodium channels available through de-inactivation, as it is thought to do in SCG
572 neurons (Liu and Bean 2014), then we expect its upregulation should prevent decay in spike height during
573 a train of spikes. Therefore, to test this prediction, we examined the ratio of the 2nd to 1st spike height of
574 multi-spiking neurons. A t-test showed that 2nd to 1st spike ratio of DB10 neurons (0.79 ± 0.03 , $n = 8$)
575 were significantly less attenuated than WT neurons (0.48 ± 0.11 , $n = 2$) ($t(8) = -4.416$, $p = 0.002$). This
576 suggests that together $K_v3.2$ and $K_v2.1$ could play a role in keeping sodium currents de-inactivated in the
577 DB10 condition.

578 DB21 neurons were significantly less excitable than both DB10 and wild type neurons: rheobase
579 was significantly increased, and input resistance was significantly reduced compared to wildtype, and
580 DB21 neurons did not produce a multi-spiking output when stimulated. DB21 neurons had significantly
581 upregulated mRNAs encoding several low threshold slow deactivating potassium currents that would be
582 expected to reduce excitability. The upregulation of *KCNA1* ($K_v1.1$) likely contributes to reduced
583 excitability given a relatively low threshold of activation (~ 32 mV) and intermediate deactivation time
584 constant (Grissmer et al. 1994). The upregulation of *KCND2* ($K_v4.2$) is consistent with the observed
585 decrease in excitability and may explain in part why the DB21 condition did not share the multispiking
586 phenotype with DB10. This is because in cultured rat superior cervical ganglion neurons, Malin and
587 Nerbonne (2000) showed that when $K_v4.2$ is overexpressed, the number of neurons displaying the multi-
588 spiking neuron phenotype is decreased, and when the gene is downregulated by expression of a dominant
589 negative transgene, there is a corresponding increase in the multi-spiking phenotype. Interestingly, the
590 authors also report increased input resistance in cells with reduced $K_v4.2$, and decreased input resistance
591 with overexpression of $K_v4.2$ (Malin and Nerbonne 2001) which is consistent with the significant
592 decrease in R_{in} in DB21 neurons.

593

594

595 *Conclusions*

596 We expected excitability of $Lepr^{db/db}$ neurons to change with increasing intensity from weeks 10
597 to 21 as diabetes progressed as diabetic neuropathy is a function of both hyperglycemia and duration in
598 humans (Maser et al. 1989; Davies et al. 2006), rats (Mattingly and Fischer 1983; Sasaki et al. 2002) and
599 mice (Giachetti 1978; Hinder et al. 2017; Liu et al. 2017). Contrary to this hypothesis, many properties
600 associated with excitability changed in 10-week animals, but were then resolved closer to wild-type levels
601 in the 21-week animals. These properties include both characteristics of intrinsic excitability (e.g.
602 probability to fire, threshold, and rebound latency) as well as many of the characteristics of the individual
603 action potentials of these neurons as well. Yet, our expression profiling of the MPGs does not simply
604 reveal a resolution at 21-weeks of changes in expression that occur in the 10-week animals. Rather, our
605 PCA reveals that the overall expression patterns in MPGs of wild type, 10-week, and 21-week animals are
606 entirely distinct. Taken together, we suggest that these results represent an apparent compensatory
607 response, where neurons of the MPG in younger diabetic mice are less adapted to hyperglycemia, or the
608 associated bladder cystopathy, than older diabetic mice that have been exposed to hyperinsulinemia for
609 longer times.

610

611

612 TABLES

613

Table 1. Non-parametric (non-normal or non-homoscedastic) negative or redundant statistical summary † Internal control that is best fit line to sampled interval. ‡ n was 27, 32, 34 for WT, DB10 and DB21 respectively.

Property (units)	WT n = 35			DB10 n = 34			DB21 n = 34			Kruskal- Wallis p =
	Mdn.	75 th per.	25 th per.	Mdn.	75 th per.	25 th per.	Mdn.	75 th per.	25 th per.	
1 st spike latency at depolarizing rheobase (ms)	14.2	17.7	10.8	13.9	17.6	12.2	15.3	18.3	11.7	0.793
1 st spike latency for Rebound spikes (-500 pA)	15.2	22.3	11.6	7.9	13.9	7.9	15.7	21.2	14.1	<0.001
Baseline slope (mV/ms) [†]	-0.3	-0.2	-0.5	-0.3	-0.1	-0.4	-0.2	-0.1	-0.4	0.424
Time from spike peak to AHP peak (ms)	8.3	11	7.3	6.9	7.5	6.1	9.8	11.2	8.1	<0.001
Spike Height (mV)	64.5	80.1	52.7	63.6	78.1	37.9	61.2	75.9	53.8	0.779
Max Spikes (spikes)	1.0	1.0	1.0	1.0	1.5	1.0	1.0	1.0	1.0	0.004
Rebound spikes (-500 pA; spikes)	1.0	1.0	1.0	1.0	1.0	1.0	1.0	1.0	1.0	0.628
Change in Membrane potential 145 ms after AP repolarization (mV) [‡]	1.8	3.8	0.9	-0.2	2.0	-0.7	0.8	1.8	0.2	0.005

614

615

616

Table 2. Negative or redundant statistical summary that was normal and homoscedastic. † Internal control that is essentially the RMP right after rebound. ‡ Redundant with area ($\frac{1}{T} \int_{t_0}^{t_0+T} Area$)

Property (units)	WT	DB10	DB21	One- way ANOVA p =
	Mean (SD) n = 35	Mean (SD) n = 34	Mean (SD) n = 34	
AP Mean Height, (mV) [‡]	1.8 (2.5)	0.7(1.7)	1.7(1.6)	0.045
Baseline (mV) [†]	-41.0 (7.8)	-41(7.6)	-38.8(5.9)	0.378

617

618 **FIGURE LEGENDS**

619 **Figure 1. Action potential properties measured from depolarization and rebound induced spikes.**

620 Each number corresponds to a given measurement, as described in the Methods. These numbers are
621 referred to in the Results section when relevant.

622 **Figure 2. *Lepr^{db/db}* mice show a strong diabetic phenotype at week 10 with hyperglycemia that is**
623 **somewhat reduced at week 21.** Diabetes associated metabolic parameters of DB vs WT mice at different
624 times; week 10 (*left*) or week 21 (*right*) in either wildtype (white) or diabetic conditions (red and green
625 for weeks 10 and week 21 respectively). **A.** A two-way ANOVA for factors genotype and age showed
626 that mouse weight was influenced by genotype and age. [Genotype; $F(1, 43) = 169.319, p < 10^{-8}$. Age; $F(1, 43) = 21.285, p = 3.5 \times 10^{-5}$. Interaction; $F(1, 43) = 3.401, p = 0.072$] **B.** A two-way ANOVA for
628 factors genotype and age showed that fasting blood glucose was influenced by genotype and age.
629 [Genotype; $F(1, 43) = 37.150, p = 2.7 \times 10^{-7}$. Age; $F(1, 43) = 8.893, p = 0.005$. Interaction; $F(1, 43) =$
630 $7.762, p = 0.008$]. **C.** Two-way ANOVA for factors genotype and age showed that fasting serum insulin
631 was influenced by genotype. [Genotype; $F(1, 43) = 71.608, p < 10^{-8}$. Age; $F(1, 43) = 0.0595, p = 0.809$.
632 Interaction; $F(1, 43) = 0.0113, p = 0.916$]. Holm-Sidak Post-Hoc test; *, $p < 0.05$; **, $p < 0.01$. Error bars
633 are SEM.

634 **Figure 3. DB10 and DB21 conditions increase and decrease excitability of MPG neurons,**
635 **respectively.** **A.** Representative traces of intracellular currents injections of -500 pA, 100 pA and 500 pA
636 current injections in WT10 (black), DB10 (red) or DB21 (green). **B. Left:** Kruskal-Wallis one way
637 ANOVA on ranks showed that rheobase was significantly altered by diabetic condition [$H(2) = 16.053, p$
638 < 0.001]. **Center:** A Kruskal-Wallis one way ANOVA on ranks showed that threshold (Figure 1, 12) was
639 significantly altered by diabetic condition [$H(2) = 9.351, p = 0.009$]. **Right:** Kruskal-Wallis one way
640 ANOVA on ranks showed that diabetic condition significantly altered latency to rebound spike [$H(2) =$
641 $22.897, p < 0.001$]. Shown are Medians, quartiles and outliers. Dunn's test; *, $p < 0.05$; **, $p < 0.01$. ***,
642 $p < 0.001$. **C. Top:** Two-way ANOVA for factors current and condition showed that cumulative

643 probability of firing 1 or more spikes as a function of injected current was reduced in DB21 condition
644 [Condition; $F(2, 1443) = 37.997$, $p < 1 \times 10^{-8}$. Current; $F(12, 1443) = 51.817$, $p < 1 \times 10^{-8}$. Interaction; F
645 $(24, 1443) = 2.038$, $p = 0.002$.]. *Bottom*: A two-way ANOVA showed that the Cumulative probability of
646 firing 2 or more spikes as a function of injected current was increased in the DB10 condition [Condition;
647 $F(2, 1443) = 43.428$, $p < 1 \times 10^{-8}$. Current; $F(12, 1443) = 2.251$, $p = 0.008$. Interaction; $F(24, 1443) =$
648 1.301 , $p = 0.150$.]. Note difference in scale. Holm-Sidak post hoc tests: $p < 0.05$; * WT10 vs DB10, †
649 WT10 vs DB21, ‡ DB10 vs DB21. Shown are Means \pm SEM.

650 **Figure 4.** Effect of condition for WT, DB10, and DB21 condition on passive properties of MPG neurons.
651 **A.** A Kruskal-Wallis one-way ANOVA on ranks showed that diabetic condition did not affect resting
652 membrane potential (RMP) [$H(2) = 2.017$, $p = 0.365$]. **B.** A Kruskal-Wallis one-way ANOVA on ranks
653 showed that diabetic condition altered input resistance (R_{in}) [$H(2) = 10.641$, $p = 0.005$] **C.** A Kruskal-
654 Wallis one way ANOVA on ranks showed that diabetic condition altered membrane time constant [$H(2)$
655 $= 6.805$, $p = 0.033$] **D.** A Kruskal-Wallis one-way ANOVA on ranks showed that diabetic condition
656 altered capacitance of MPG neurons [$H(2) = 23.187$, $p < 0.001$]. Data shown are medians, quartiles and
657 outliers. Dunn's test: * $p < 0.05$; **, $p < 0.01$.

658 **Figure 5. Action potential (AP) parameters are altered by DB condition in mouse MPG neurons.** AP
659 properties illustrated in figure 1 were quantified in 10 week wildtype (Black), 10 week Diabetic (Red) and
660 21 week diabetic (Green) in mouse MPG neurons. All data except A were quantified from rebound
661 spikes. **A.** A Kruskal-Wallis one way ANOVA on ranks showed that diabetic condition affected
662 ascending spike slope elicited by depolarizing current injection (Figure 1, 9) during depolarizing current
663 injection of MPG neurons [$H(2) = 22.010$, $p < 0.001$]. **B.** A Kruskal-Wallis one way ANOVA on ranks
664 showed that diabetic condition affected AP half-width (Figure 1, 3) [$H(2) = 14.892$, $p < 0.001$]. **C.** A
665 Kruskal-Wallis one way ANOVA on ranks showed that diabetic condition did not significantly alter AP
666 maximum rise slope (Figure 1, 10) [$H(2) = 5.670$, $p = 0.059$]. **D.** A Kruskal-Wallis one way ANOVA on
667 ranks showed that diabetic condition altered maximum AP decay slope of (Figure 1, 11) [$H(2) = 8.112$, p

668 = 0.017]. **E.** A Kruskal-Wallis one way ANOVA on ranks showed that diabetic condition altered AP 10-
669 90% rise time (Figure 1, 4) [$H(2) = 6.464, p = 0.039$]. **F.** A Kruskal-Wallis one way ANOVA on ranks
670 showed that diabetic condition altered 90-10% decay time (Figure 1, 5) [$H(2) = 42.223, p < 0.001$]. **G.** A
671 Kruskal-Wallis one way ANOVA on ranks showed that diabetic condition did not alter AP 10-90% rise
672 slope (Figure 1, 7) [$H(2) = 2.043, p = 0.360$]. **H.** A one-way ANOVA showed that diabetic condition
673 altered 90-10% decay slope (Figure 1, 8) [$F(2, 101) = 11.541, p = 3.1 \times 10^{-5}$]. **I.** A Kruskal-Wallis one-
674 way ANOVA on ranks showed that diabetic condition altered AP area (Figure 1, 6) [$H(2) = 12.320, p =$
675 0.002]. **J.** A Kruskal-Wallis one-way ANOVA on ranks showed that diabetic condition did not alter AHP
676 area (Figure 1, 13) [$H(2) = 0.530, p = 0.767$]. **K.** A Kruskal-Wallis one-way ANOVA on ranks showed
677 that diabetic condition did not alter AHP amplitude (Figure 1, 2) [$H(2) = 2.900, p = 0.235$]. **L.** A
678 Kruskal-Wallis one way ANOVA on ranks showed that diabetic condition altered AHP decay tau (Figure
679 1, 14) [$H(2) = 11.896, p = 0.003$]. Data shown are medians, quartiles and outliers. Dunn's test: * $p <$
680 0.05 ; **, $p < 0.01$.

681 **Figure 6. mRNA copy numbers for ion channel subunits of across WT, DB10, and DB21**

682 **experimental groups.** Significant differences as noted ($p < 0.05$; post-hoc Holm-Šídák analyses
683 following One-Way ANOVA) represent pairwise comparisons across all three groups. Data shown are
684 medians, quartiles and each individual value from a given animal.

685 **Figure 7. Principal components analysis (PCA) of spike characteristic across WT, DB10, and DB21**

686 **mice. A.** The first two principal components (PC1 and PC2) define the x-and y-axes respectively. PC1
687 accounted for 42.5% of the variance while PC2 accounted for 14.6%. By and large, all three groups show
688 overlapping distribution of variance across PC1 and PC2. **B.** Scree plot demonstrating the amount of
689 variance accounted for across the first 10 principal components. A substantial plurality of the variance is
690 accounted for in the first principal component, while the remainder contribute far less to the variance in
691 the data. **C.** Post-hoc analysis of the variables that contribute to the variance in PC1 reveals that relatively
692 equal contributions are found from variables associated with spike shape and AHP amplitude.

693 **Figure 8. PCA of ion channel mRNA levels across WT, DB10, and DB21 mice. A.** The first two
694 principal components (PC1 and PC2) define the x-and y-axes respectively. PC1 accounted for 25.6% of
695 the variance while PC2 accounted for 21.9%. The distribution across PC1 and PC2 reveals three distinct
696 ion channel expression profiles for WT, DB10, and DB21 animals. **B.** Scree plot demonstrating the
697 amount of variance accounted for across the first 10 principal components. The majority of the variance is
698 accounted for in the PC1 and PC2, while the remainder contribute far less to the variance in the data. **C.**
699 Post-hoc analysis of the variables that contribute to the variance in PC1 and PC2 reveals distinct channel
700 subunits that account for the distinct patterns of expression seen in all three experimental groups.

701

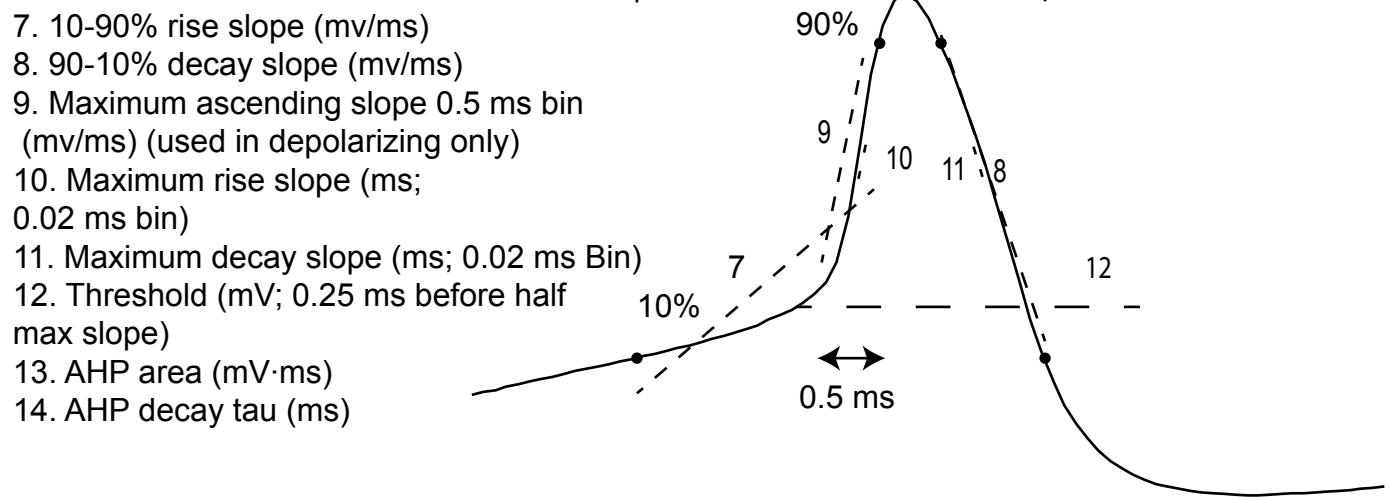
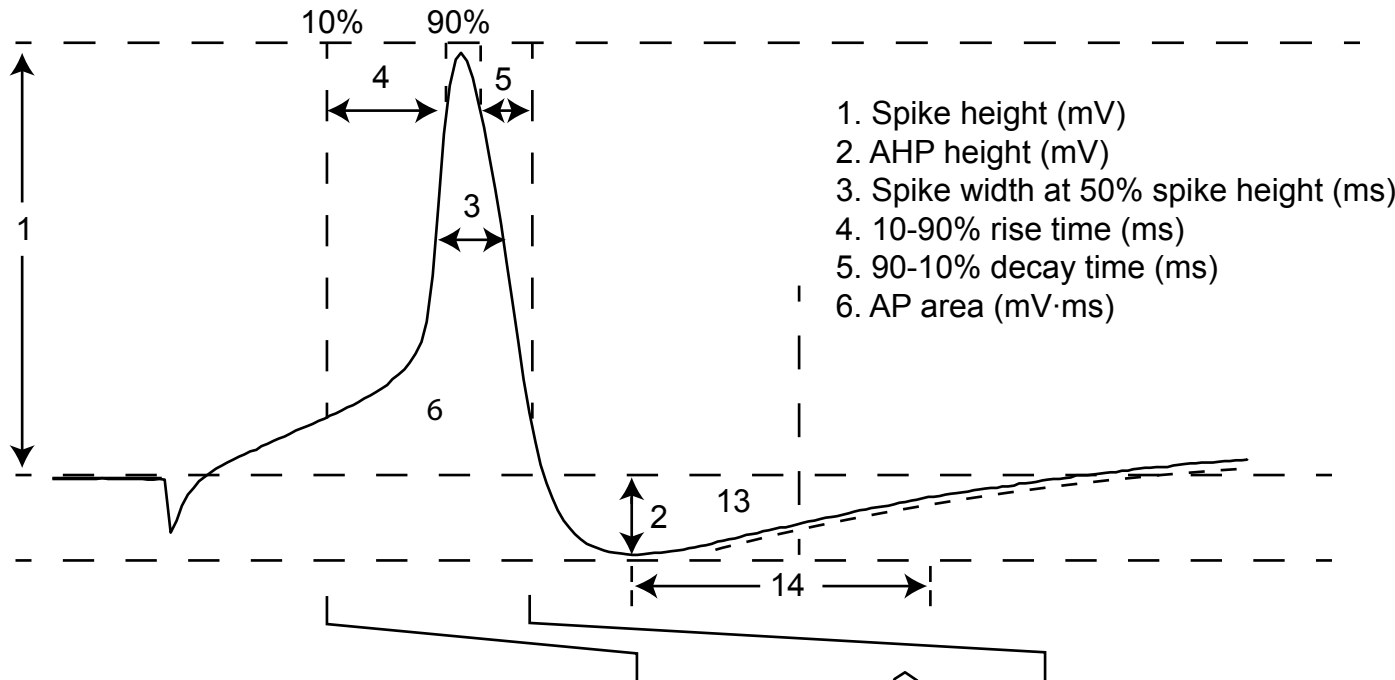
702 **REFERENCES**

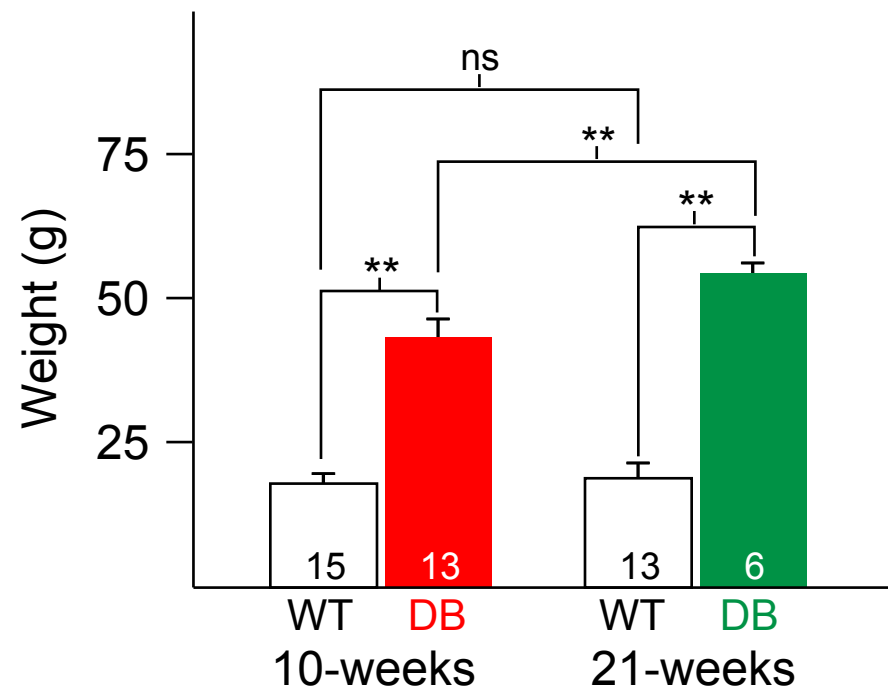
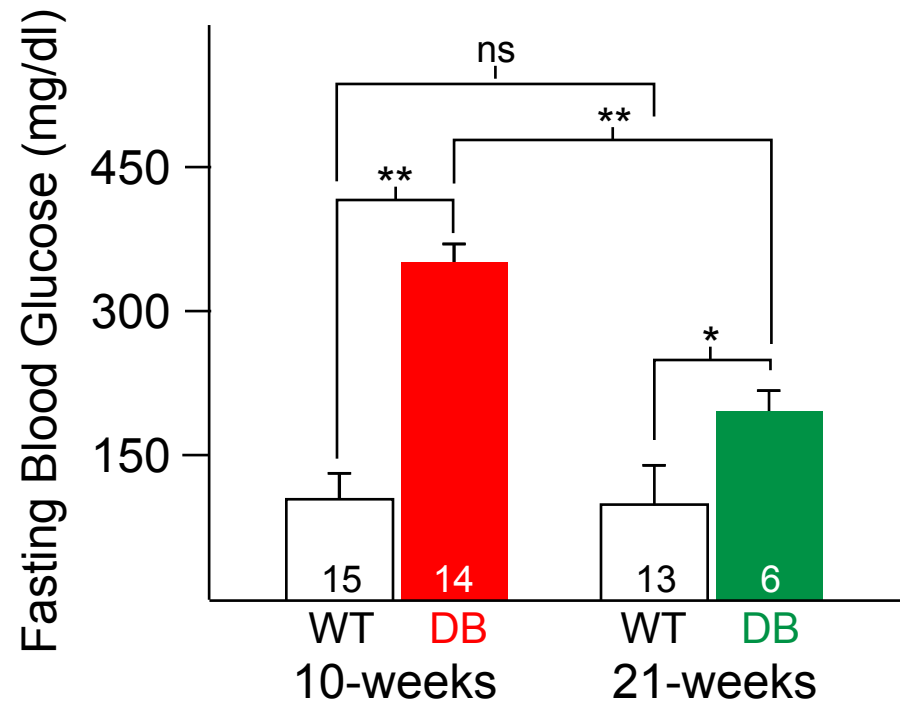
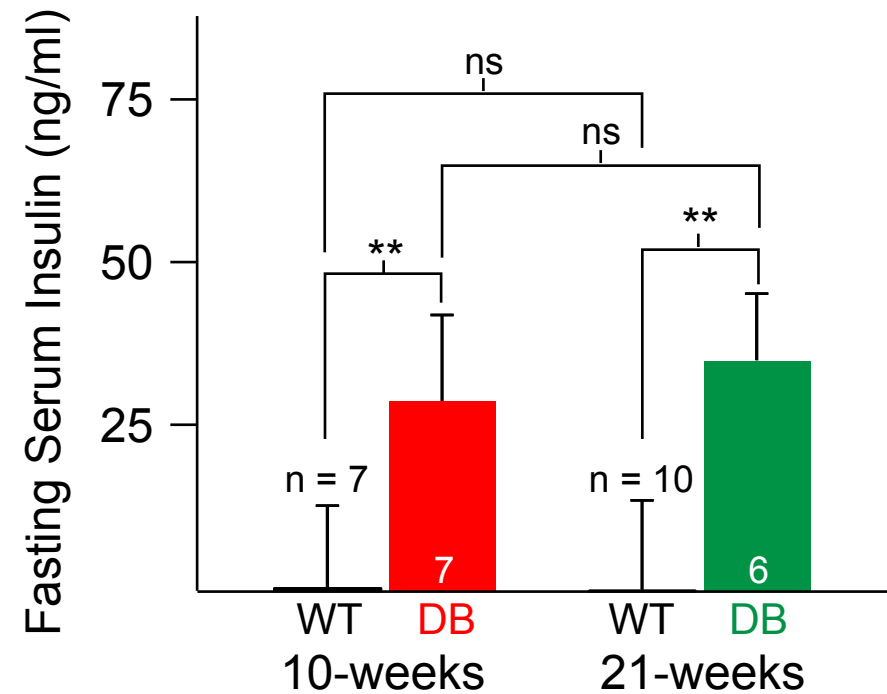
- 703 **Breyer MD, Bottinger E, Brosius 3rd FC, Coffman TM, Harris RC, Heilig CW, Sharma K, Amdcc.**
704 Mouse models of diabetic nephropathy. *J Am Soc Nephrol* 16: 27–45, 2005.
- 705 **Cassell JF, Clark AL, McLachlan EM.** Characteristics of phasic and tonic sympathetic ganglion cells of
706 the guinea-pig [Online]. *J Physiol* 372: 457–483, 1986. <http://www.ncbi.nlm.nih.gov/pubmed/2425087>.
- 707 **Chen H, Charlat O, Tartaglia LA, Woolf EA, Weng X, Ellis SJ, Lakey ND, Culpepper J, Moore KJ,**
708 **Breitbart RE, Duyk GM, Tepper RI, Morgenstern JP.** Evidence that the diabetes gene encodes the
709 leptin receptor: identification of a mutation in the leptin receptor gene in db/db mice [Online]. *Cell* 84:
710 491–495, 1996. <http://www.ncbi.nlm.nih.gov/pubmed/8608603>.
- 711 **Daneshgari F, Huang X, Liu G, Bena J, Saffore L, Powell CT.** Temporal differences in bladder
712 dysfunction caused by diabetes, diuresis, and treated diabetes in mice. *Am J Physiol Regul Integr Comp*
713 *Physiol* 290: R1728–35, 2006a.
- 714 **Daneshgari F, Liu G, Imrey PB.** Time Dependent Changes in Diabetic Cystopathy in Rats Include
715 Compensated and Decompensated Bladder Function. *J Urol* 176: 380–386, 2006b.
- 716 **Davies M, Brophy S, Williams R, Taylor A.** The prevalence, severity, and impact of painful diabetic
717 peripheral neuropathy in type 2 diabetes. *Diabetes Care* 29: 1518–1522, 2006.
- 718 **DCCT Research Group the.** The absence of a glycemic threshold for the development of long-term
719 complications: the perspective of the Diabetes Control and Complications Trial [Online]. *Diabetes* 45:
720 1289–1298, 1996. <http://www.ncbi.nlm.nih.gov/pubmed/8826962>.
- 721 **Faerman I, Maler M, Jadzinsky M, Alvarez E, Fox D, Zilbervarg J, Cibeira JB, Colinas R.**
722 Asymptomatic neurogenic bladder in juvenile diabetics [Online]. *Diabetologia* 7: 168–172, 1971.
723 <http://www.ncbi.nlm.nih.gov/pubmed/5560918>.
- 724 **Frimodt-Moller C.** Diabetic cystopathy: epidemiology and related disorders [Online]. *Ann Intern Med*
725 92: 318–321, 1980. <http://www.ncbi.nlm.nih.gov/pubmed/7356221>.
- 726 **Garcia VB, Abbinati MD, Harris-Warrick RM, Schulz DJ.** Effects of chronic spinal cord injury on
727 relationships among ion channel and receptor mRNAs in mouse lumbar spinal cord. *Neuroscience*
728 submitted, 2018.
- 729 **Garcia VB, Garcia ML, Schulz DJ.** Quantitative expression profiling in mouse spinal cord reveals
730 changing relationships among channel and receptor mRNA levels across postnatal maturation.
731 *Neuroscience* 277: 321–333, 2014.
- 732 **Giachetti A.** The functional state of sympathetic nerves in spontaneously diabetic mice [Online].
733 *Diabetes* 27: 969–974, 1978. <http://www.ncbi.nlm.nih.gov/pubmed/700260>.
- 734 **Golowasch J, Thomas G, Taylor AL, Patel A, Pineda A, Khalil C, Nadim F.** Membrane capacitance
735 measurements revisited: dependence of capacitance value on measurement method in nonisopotential
736 neurons. *J Neurophysiol* 102: 2161–2175, 2009.
- 737 **Grissmer S, Nguyen AN, Aiyar J, Hanson DC, Mather RJ, Gutman GA, Karmilowicz MJ, Auperin**
738 **DD, Chandy KG.** Pharmacological characterization of five cloned voltage-gated K⁺ channels, types
739 Kv1.1, 1.2, 1.3, 1.5, and 3.1, stably expressed in mammalian cell lines [Online]. *Mol Pharmacol* 45:
740 1227–1234, 1994. <http://www.ncbi.nlm.nih.gov/pubmed/7517498>.
- 741 **Gunnarsson R.** Function of the pancreatic B-cell during the development of hyperglycaemia in mice

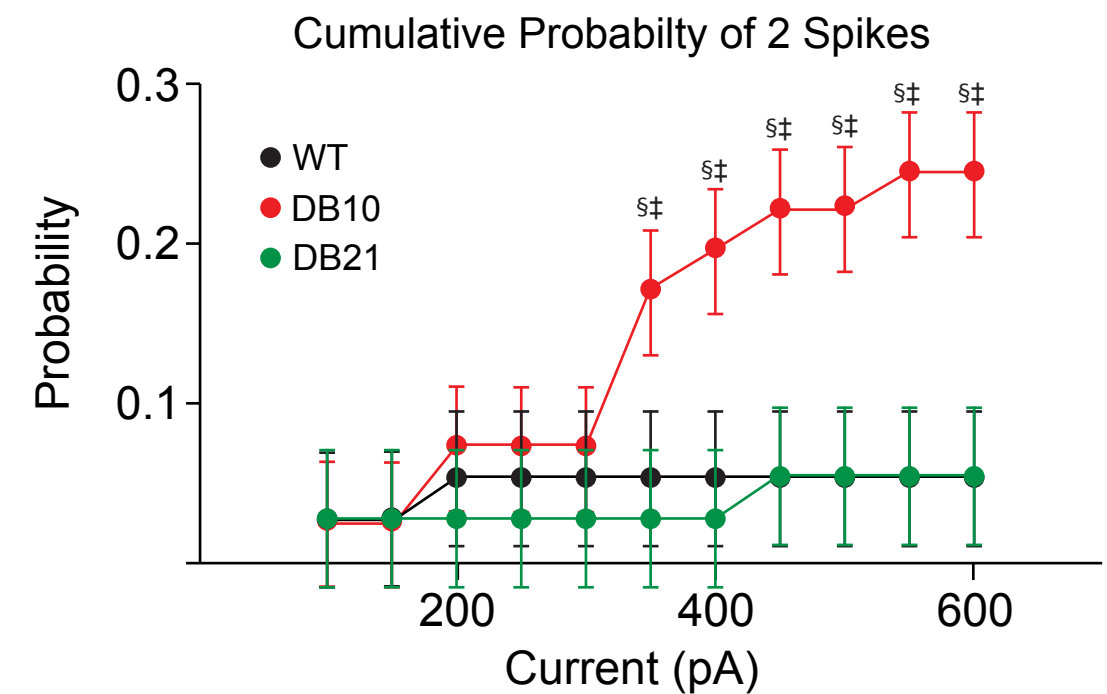
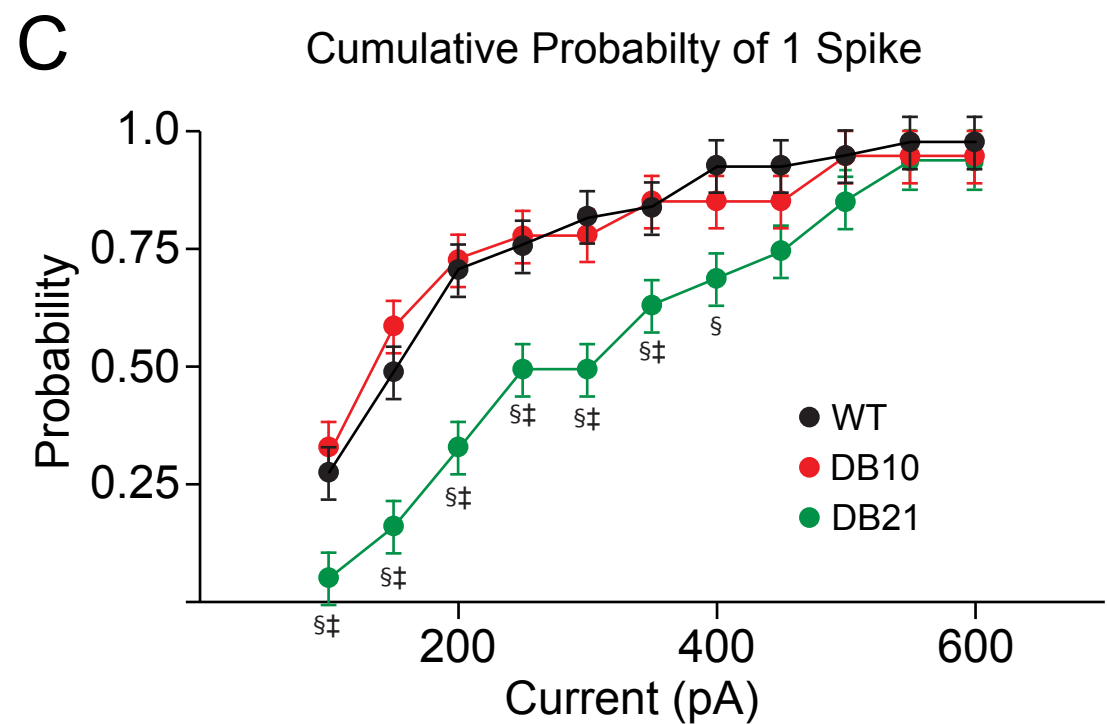
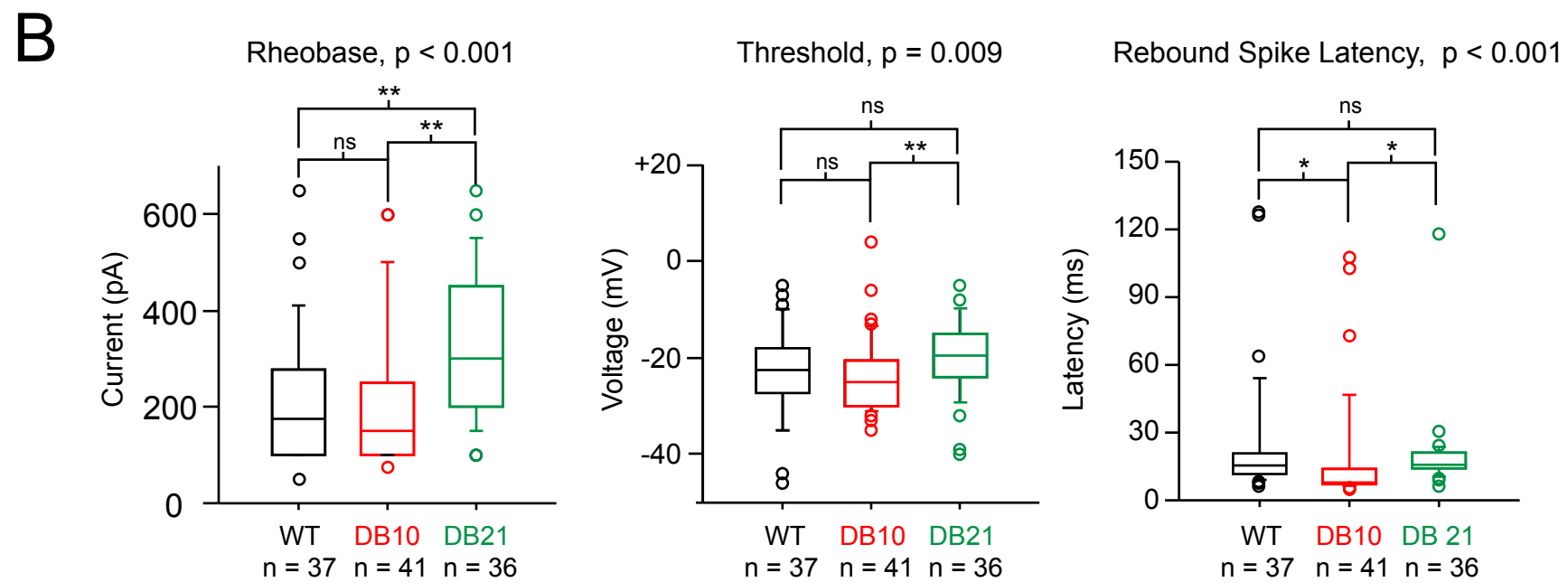
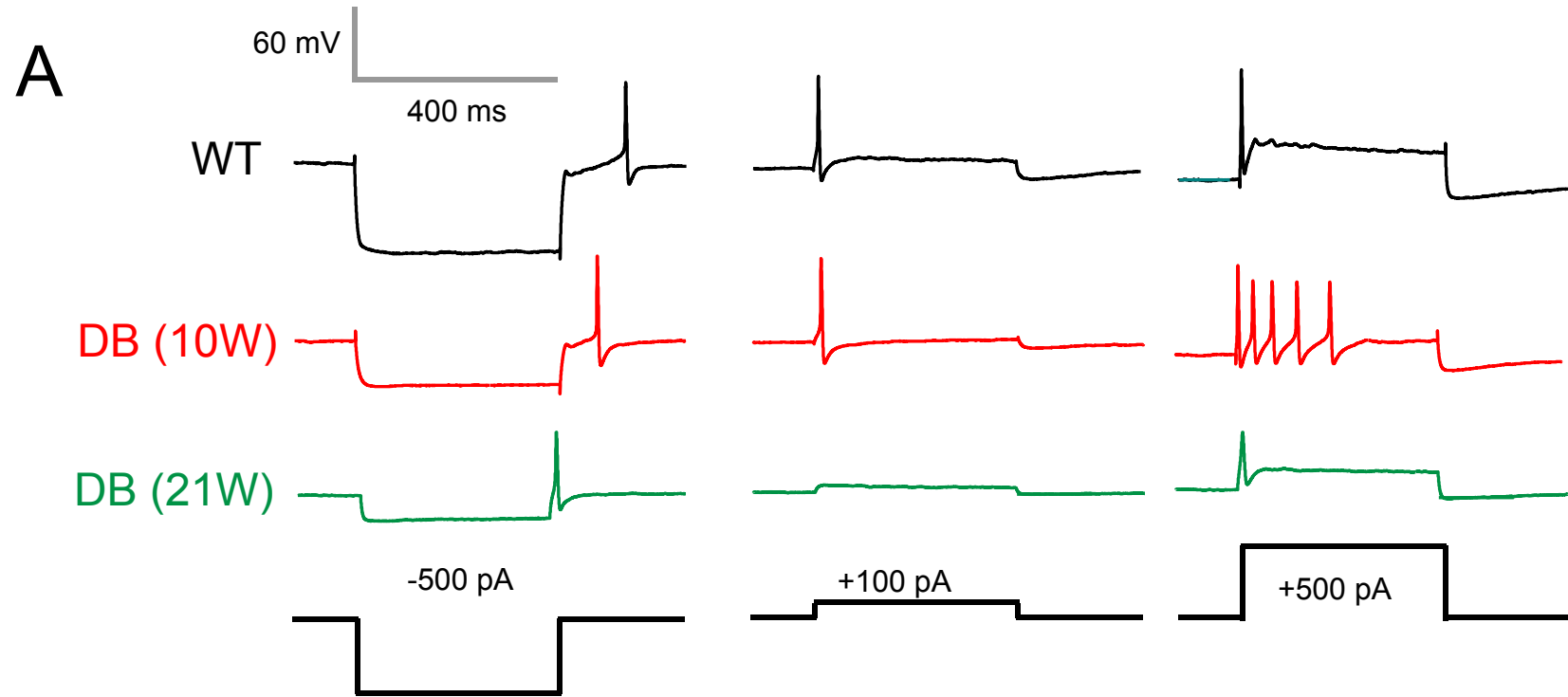
- 742 homozygous for the mutations “diabetes” (db) and “misty” (m) [Online]. *Diabetologia* 11: 431–438,
743 1975. <http://www.ncbi.nlm.nih.gov/pubmed/1103367>.
- 744 **Hanani M.** Satellite glial cells in sympathetic and parasympathetic ganglia: in search of function. *Brain*
745 *Res Rev* 64: 304–327, 2010.
- 746 **Hinder LM, O’Brien PD, Hayes JM, Backus C, Solway AP, Sims-Robinson C, Feldman EL.** Dietary
747 reversal of neuropathy in a murine model of prediabetes and metabolic syndrome. *Dis Model Mech* 10:
748 717–725, 2017.
- 749 **Hummel KP, Coleman DL, Lane PW.** The influence of genetic background on expression of mutations
750 at the diabetes locus in the mouse. I. C57BL-KsJ and C57BL-6J strains [Online]. *Biochem Genet* 7: 1–13,
751 1972. <http://www.ncbi.nlm.nih.gov/pubmed/4557514>.
- 752 **Isom LL, Scheuer T, Brownstein AB, Ragsdale DS, Murphy BJ, Catterall WA.** Functional co-
753 expression of the beta 1 and type IIA alpha subunits of sodium channels in a mammalian cell line. *J Biol*
754 *Chem* 270: 3306–12, 1995.
- 755 **Kaplan SA, Te AE, Blaivas JG.** Urodynamic findings in patients with diabetic cystopathy [Online]. *J*
756 *Urol* 153: 342–344, 1995. <http://www.ncbi.nlm.nih.gov/pubmed/7815578>.
- 757 **Kebapci N, Yenilmez A, Efe B, Entok E, Demirustu C.** Bladder dysfunction in type 2 diabetic patients.
758 *Neurourol Urodyn* 26: 814–819, 2007.
- 759 **Lee J-H, Kim E-G, Park B-G, Kim K-H, Cha S-K, Kong ID, Lee J-W, Jeong S-W.** Identification of
760 T-Type $\alpha 1H$ Ca²⁺ Channels (Ca_v 3.2) in Major Pelvic Ganglion Neurons. *J Neurophysiol* 87: 2844–2850,
761 2002.
- 762 **Liu PW, Bean BP.** Kv2 channel regulation of action potential repolarization and firing patterns in
763 superior cervical ganglion neurons and hippocampal CA1 pyramidal neurons. *J Neurosci* 34: 4991–5002,
764 2014.
- 765 **Liu Y, Sebastian B, Liu B, Zhang Y, Fissel JA, Pan B, Polydefkis M, Farah MH.** Sensory and
766 autonomic function and structure in footpads of a diabetic mouse model. *Sci Rep* 7: 41401, 2017.
- 767 **Malin SA, Nerbonne JM.** Molecular heterogeneity of the voltage-gated fast transient outward K⁺
768 current, I(Af), in mammalian neurons [Online]. *J Neurosci* 21: 8004–8014, 2001.
769 <http://www.ncbi.nlm.nih.gov/pubmed/11588173>.
- 770 **Maser RE, Steenkiste AR, Dorman JS, Nielsen VK, Bass EB, Manjoo Q, Drash AL, Becker DJ,**
771 **Kuller LH, Greene DA, et al.** Epidemiological correlates of diabetic neuropathy. Report from Pittsburgh
772 Epidemiology of Diabetes Complications Study [Online]. *Diabetes* 38: 1456–1461, 1989.
773 <http://www.ncbi.nlm.nih.gov/pubmed/2620781>.
- 774 **Mattingly GE, Fischer VW.** Peripheral neuropathy following prolonged exposure to streptozotocin-
775 induced diabetes in rats: a teased nerve fiber study [Online]. *Acta Neuropathol* 59: 133–138, 1983.
776 <http://www.ncbi.nlm.nih.gov/pubmed/6301203>.
- 777 **Medici F, Hawa M, Ianari A, Pyke DA, Leslie RD.** Concordance rate for type II diabetes mellitus in
778 monozygotic twins: actuarial analysis. *Diabetologia* 42: 146–150, 1999.
- 779 **Metz AE, Jarsky T, Martina M, Spruston N.** R-Type Calcium Channels Contribute to
780 Afterdepolarization and Bursting in Hippocampal CA1 Pyramidal Neurons [Online]. *J Neurosci* 25, 2005.
781 <http://www.jneurosci.org/content/25/24/5763/tab-figures-data> [25 Jun. 2018].
- 782 **Nadelhaft I, Vera PL.** Reduced urinary bladder afferent conduction velocities in streptozocin diabetic

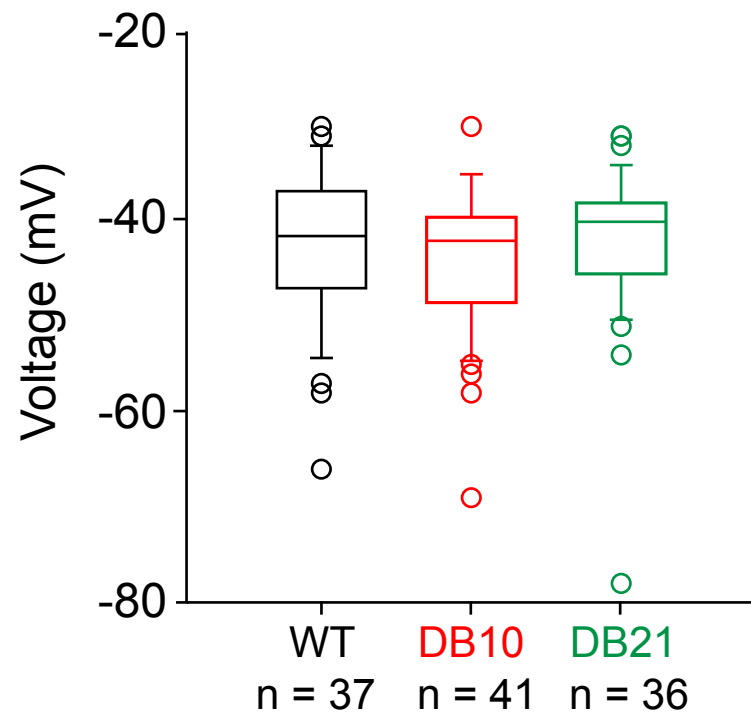
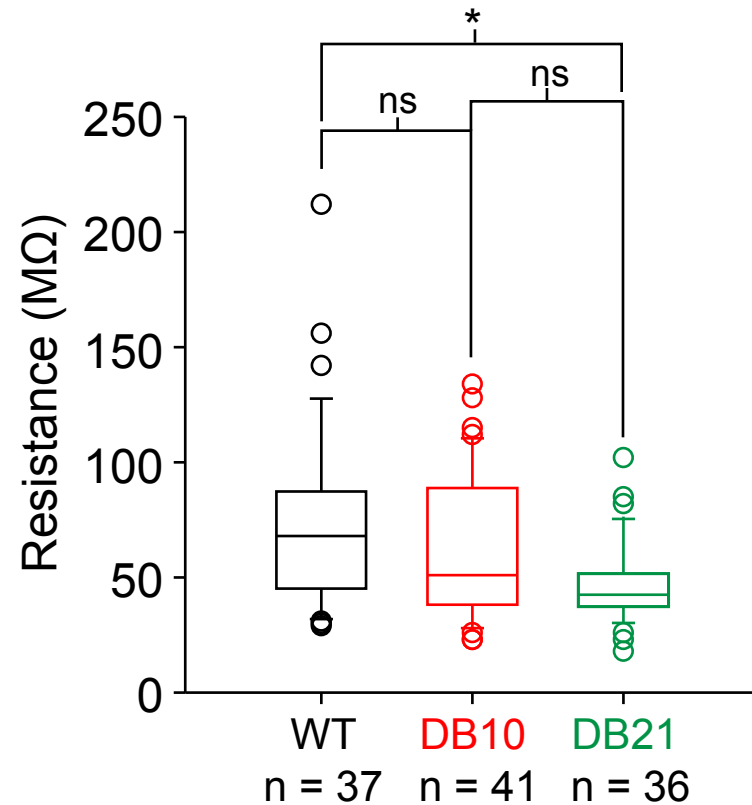
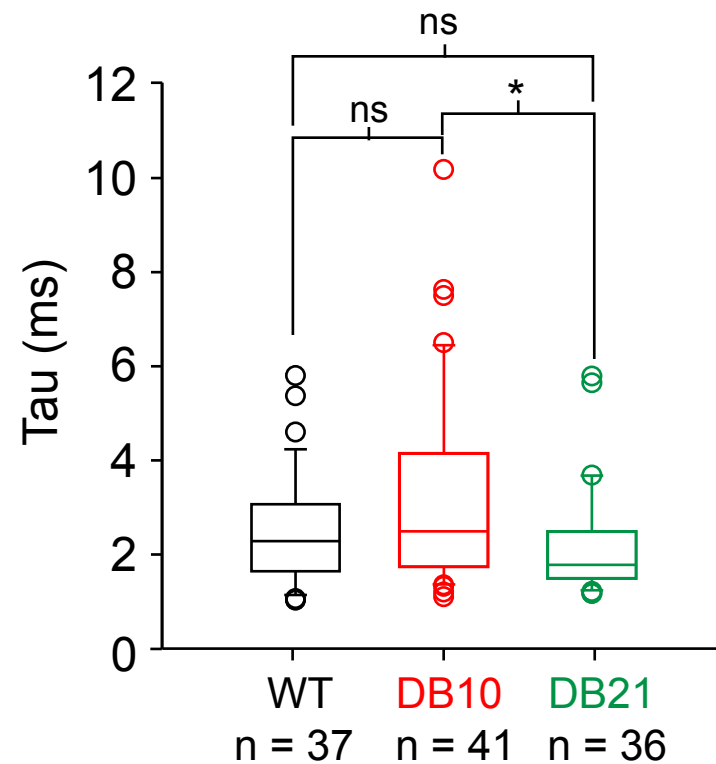
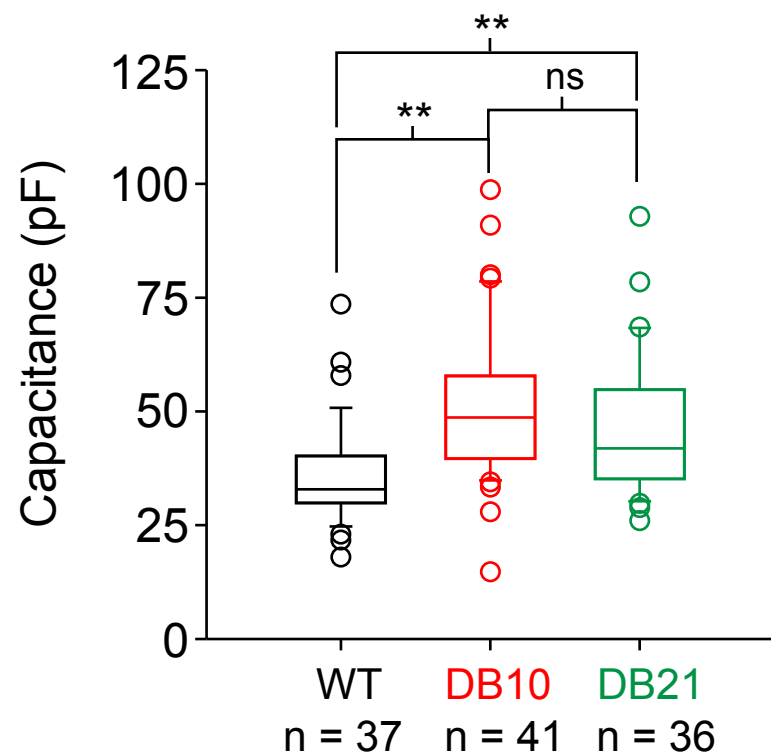
- 783 rats [Online]. *Neurosci Lett* 135: 276–278, 1992. <http://www.ncbi.nlm.nih.gov/pubmed/1625809>.
- 784 **Naundorf B, Wolf F, Volgushev M.** Unique features of action potential initiation in cortical neurons.
785 *Nature* 440: 1060–1063, 2006.
- 786 **Perez-Reyes E.** Molecular Physiology of Low-Voltage-Activated T-type Calcium Channels. *Physiol Rev*
787 83: 117–161, 2003.
- 788 **Platkiewicz J, Brette R.** A threshold equation for action potential initiation. *PLoS Comput Biol* 6:
789 e1000850, 2010.
- 790 **Platkiewicz J, Brette R.** Impact of fast sodium channel inactivation on spike threshold dynamics and
791 synaptic integration. *PLoS Comput Biol* 7: e1001129, 2011.
- 792 **Rudy B, McBain CJ.** Kv3 channels: voltage-gated K⁺ channels designed for high-frequency repetitive
793 firing [Online]. *Trends Neurosci* 24: 517–526, 2001. <http://www.ncbi.nlm.nih.gov/pubmed/11506885>.
- 794 **Sasaki K, Chancellor MB, Goins WF, Phelan MW, Glorioso JC, de Groat WC, Yoshimura N.** Gene
795 therapy using replication-defective herpes simplex virus vectors expressing nerve growth factor in a rat
796 model of diabetic cystopathy [Online]. *Diabetes* 53: 2723–2730, 2004.
797 <http://www.ncbi.nlm.nih.gov/pubmed/15448108>.
- 798 **Sasaki K, Chancellor MB, Phelan MW, Yokoyama T, Fraser MO, Seki S, Kubo K, Kumon H,**
799 **Groat WC, Yoshimura N.** Diabetic cystopathy correlates with a long-term decrease in nerve growth
800 factor levels in the bladder and lumbosacral dorsal root Ganglia. *J Urol* 168: 1259–1264, 2002.
- 801 **Springer MG, Kullmann PH, Horn JP.** Virtual leak channels modulate firing dynamics and synaptic
802 integration in rat sympathetic neurons: implications for ganglionic transmission in vivo. *J Physiol* 593:
803 803–823, 2015.
- 804 **Sullivan KA, Hayes JM, Wiggin TD, Backus C, Su Oh S, Lentz SI, Brosius 3rd F, Feldman EL.**
805 Mouse models of diabetic neuropathy. *Neurobiol Dis* 28: 276–285, 2007.
- 806 **Suzuki S, Rogawski MA.** T-type calcium channels mediate the transition between tonic and phasic firing
807 in thalamic neurons [Online]. *Proc Natl Acad Sci U S A* 86: 7228–7232, 1989.
808 <http://www.ncbi.nlm.nih.gov/pubmed/2550936>.
- 809 **Tompkins JD, Vizzard MA, Parsons RL.** Synaptic transmission at parasympathetic neurons of the
810 major pelvic ganglion from normal and diabetic male mice. *J Neurophysiol* 109: 988–995, 2013.
- 811 **UKPDS.** Intensive blood-glucose control with sulphonylureas or insulin compared with conventional
812 treatment and risk of complications in patients with type 2 diabetes (UKPDS 33). UK Prospective
813 Diabetes Study (UKPDS) Group [Online]. *Lancet* 352: 837–853, 1998.
814 <http://www.ncbi.nlm.nih.gov/pubmed/9742976>.
- 815 **United States. Department of Health and Human Services., Center for Disease Control., National**
816 **Center for Health Statistics (U.S.).** Health, United States, 2016□: with chartbook on Long-term Trends
817 in Health [Online]. Hyattsville, MD: National Center for Health Statistics.
818 <https://www.cdc.gov/nchs/data/hs/hs16.pdf>.
- 819 **Vacher H, Mohapatra DP, Trimmer JS.** Localization and Targeting of Voltage-Dependent Ion
820 Channels in Mammalian Central Neurons. *Physiol Rev* 88: 1407–1447, 2008.
- 821 **Vandesompele J, De Preter K, Pattyn I, Poppe B, Van Roy N, De Paepe A, Speleman R.** Accurate
822 normalization of real-time quantitative RT-PCR data by geometric averaging of multiple internal control
823 genes. *Genome Biol* 3: research0034.1–0034.11, 2002.

- 824 **Vinik AI, Maser RE, Mitchell BD, Freeman R.** Diabetic autonomic neuropathy [Online]. *Diabetes*
825 *Care* 26: 1553–1579, 2003. <http://www.ncbi.nlm.nih.gov/pubmed/12716821>.
- 826 **Vinik AI, Maser RE, Ziegler D.** Autonomic imbalance: prophet of doom or scope for hope? *Diabet Med*
827 28: 643–651, 2011.
- 828 **Wang B, Chandrasekera PC, Pippin JJ.** Leptin- and leptin receptor-deficient rodent models: relevance
829 for human type 2 diabetes [Online]. *Curr Diabetes Rev* 10: 131–145, 2014.
830 <http://www.ncbi.nlm.nih.gov/pubmed/24809394>.
- 831 **Weiser M, Vega-Saenz de Miera E, Kentros C, Moreno H, Franzen L, Hillman D, Baker H, Rudy**
832 **B.** Differential expression of Shaw-related K⁺ channels in the rat central nervous system [Online]. *J*
833 *Neurosci* 14: 949–972, 1994. <http://www.ncbi.nlm.nih.gov/pubmed/8120636>.
- 834 **White WE, Hooper SL.** Contamination of current-clamp measurement of neuron capacitance by voltage-
835 dependent phenomena. *J Neurophysiol* 110: 257–268, 2013.
- 836 **Won YJ, Whang K, Kong ID, Park KS, Lee JW, Jeong SW.** Expression profiles of high voltage-
837 activated calcium channels in sympathetic and parasympathetic pelvic ganglion neurons innervating the
838 urogenital system. *J Pharmacol Exp Ther* 317: 1064–1071, 2006.
- 839 **Yuan Z, Tang Z, He C, Tang W.** Diabetic cystopathy: A review. *J Diabetes* 7: 442–447, 2015.
- 840
- 841

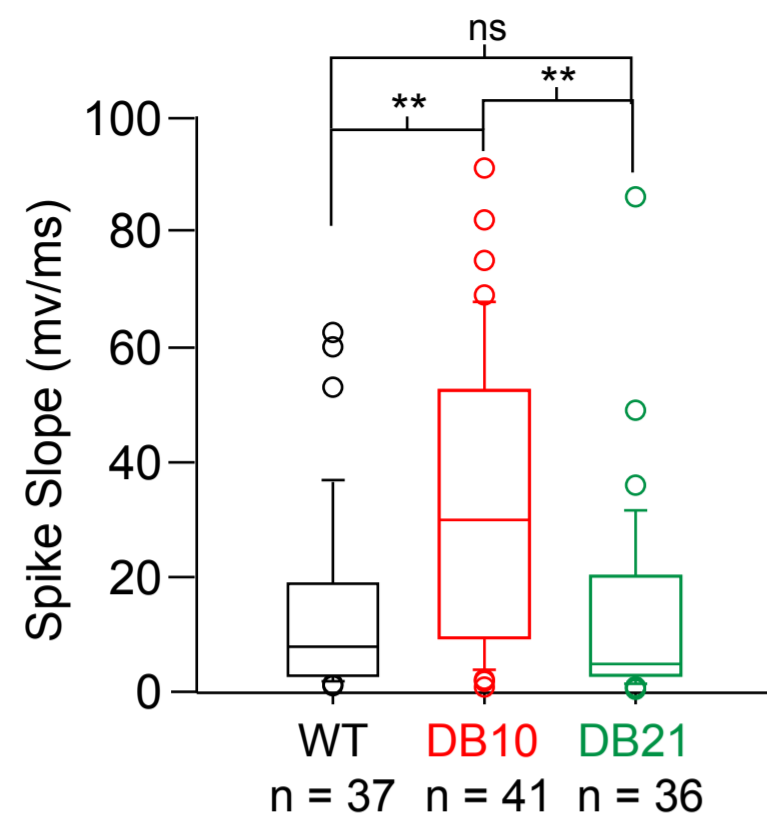


A**Weight****B****Fasting Blood Glucose****C****Fasting Serum Insulin**

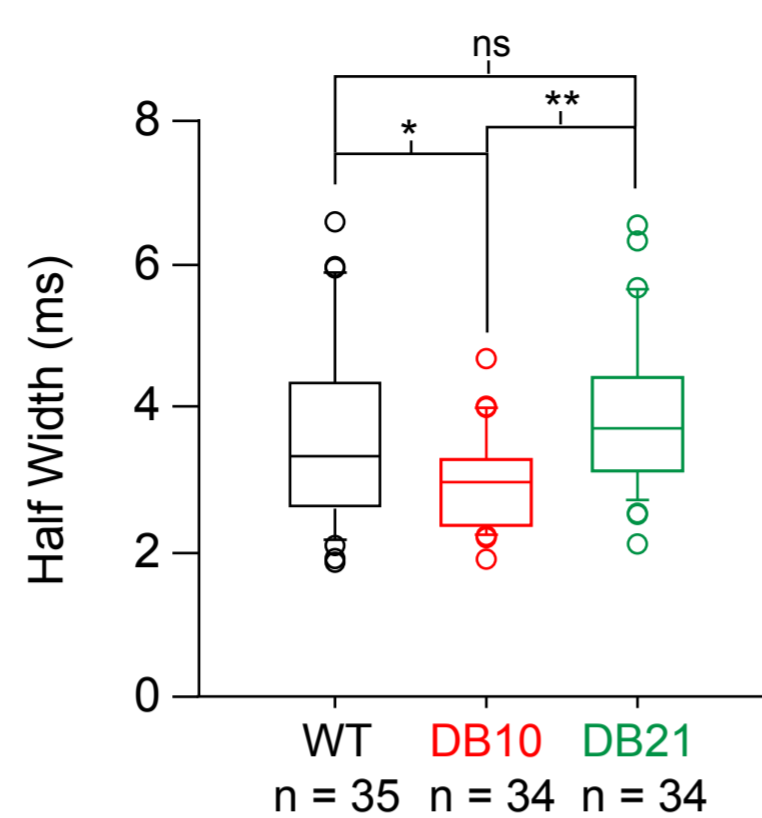


AResting Membrane Potential, $p = 0.365$ **B** R_{in} , $p = 0.005$ **C**Tau, $p = 0.033$ **D**Capacitance, $p < 0.001$ 

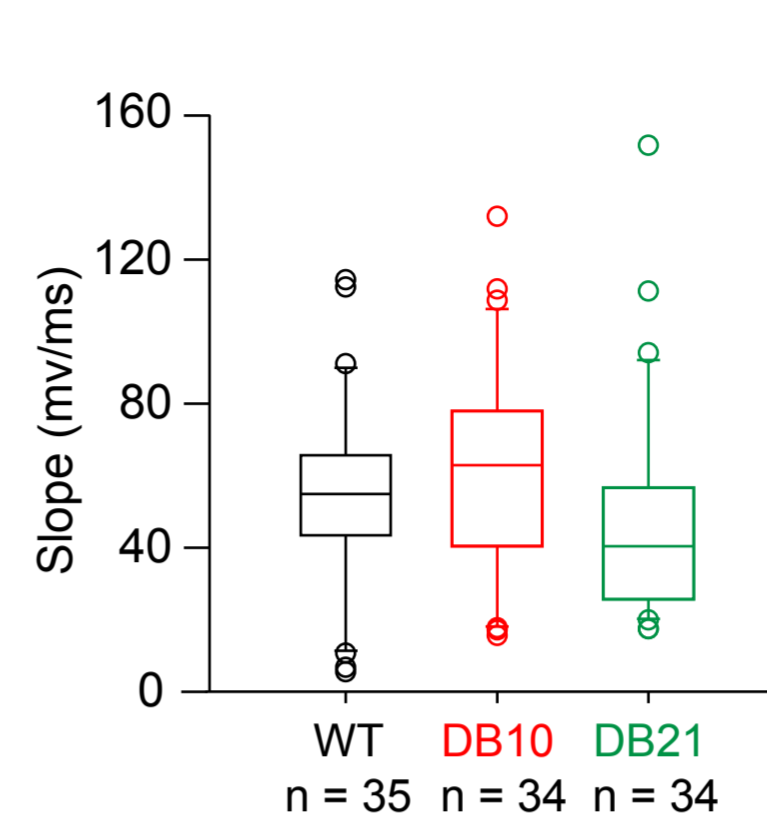
A Spike Slope Ascending (depolarizing), $p < 0.001$



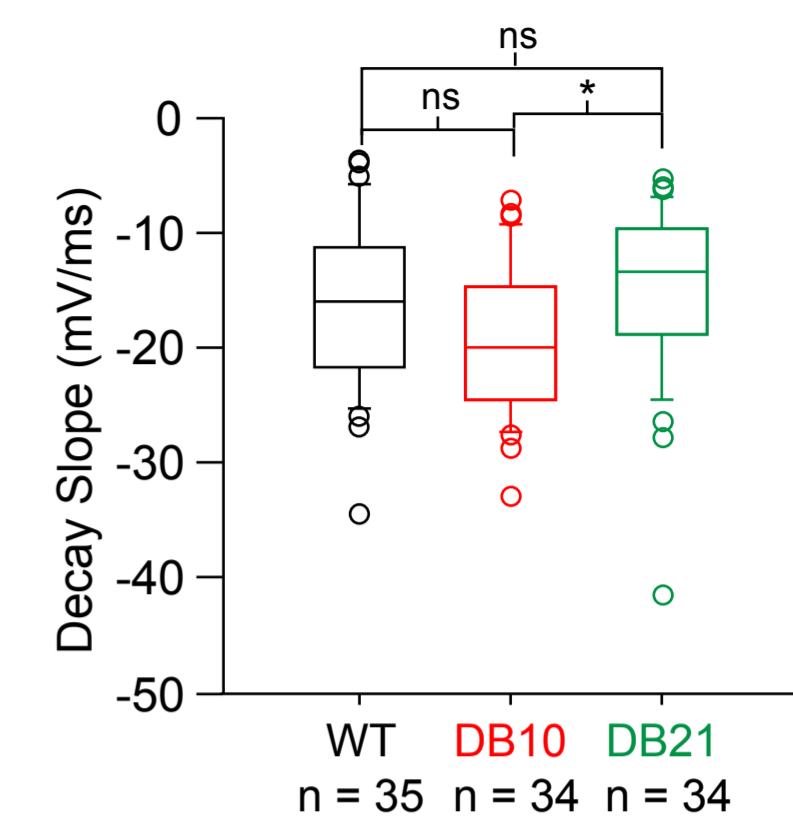
B Half-Width, $p < 0.001$



C Max Rise Slope (rebound), $p = 0.059$

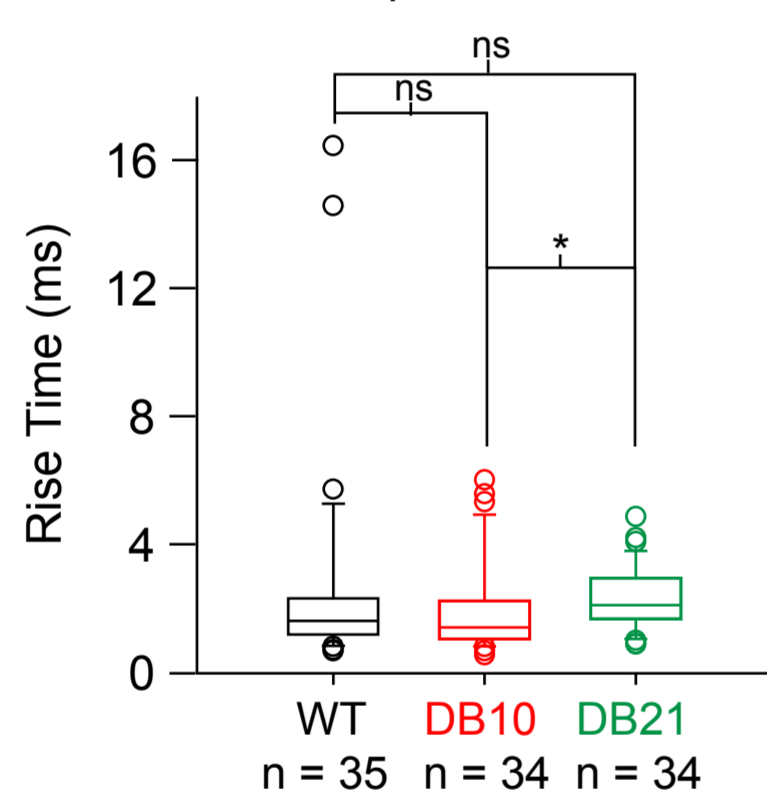


D Max Decay Slope (Rebound), $p = 0.016$

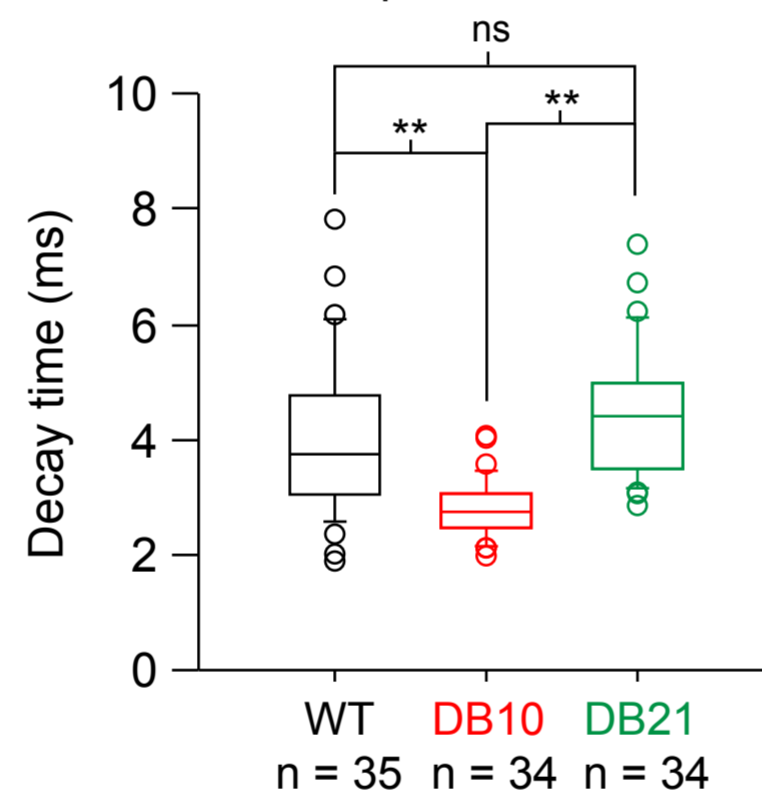


bioRxiv preprint doi: <https://doi.org/10.1101/360826>; this version posted July 6, 2018. The copyright holder for this preprint (which was not certified by peer review) is the author/funder, who has granted bioRxiv a license to display the preprint in perpetuity. It is made available under aCC-BY-NC-ND 4.0 International license.

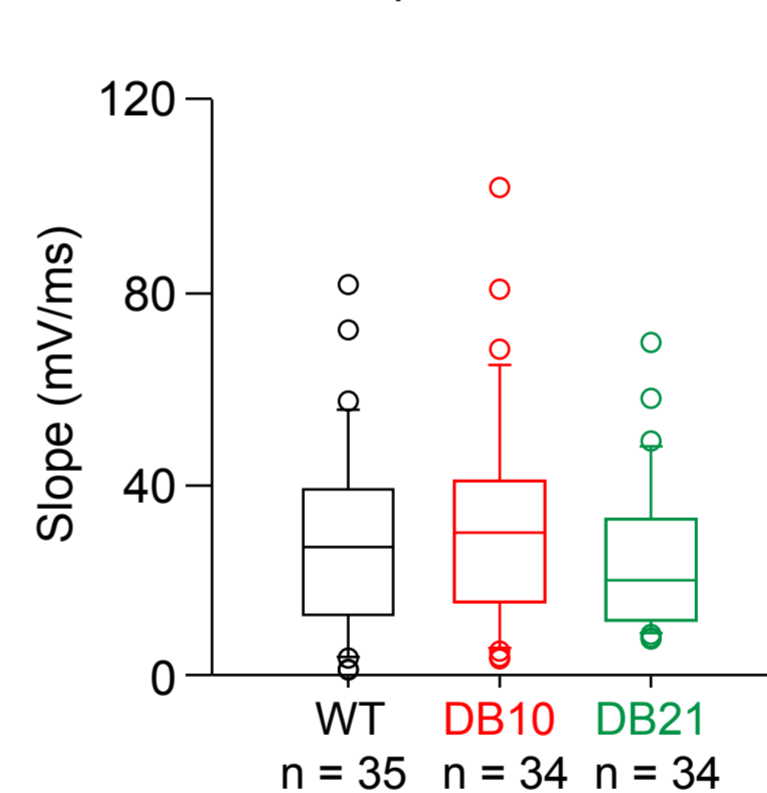
E 10-90% Rise Time, $p = 0.039$



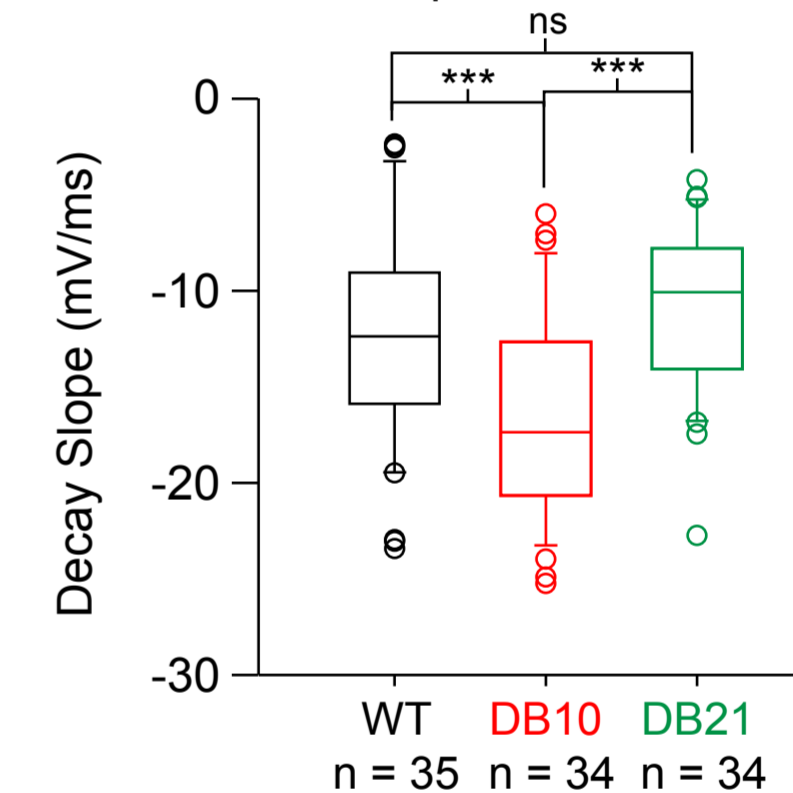
F 90-10% Decay time, $p < 0.001$



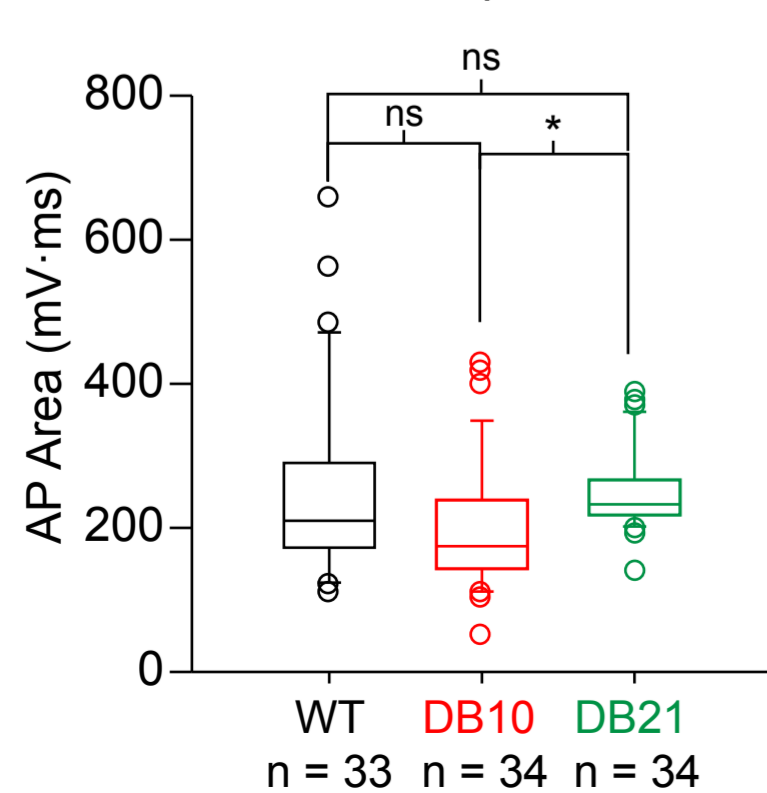
G 10-90% Rise Slope, $p = 0.360$



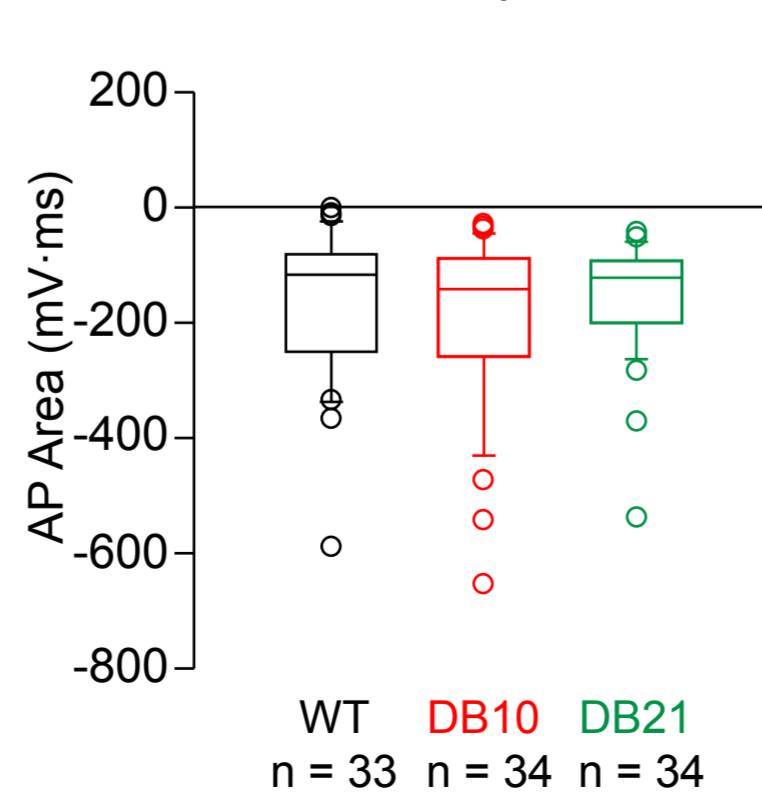
H 90-10% Decay slope, $p < 0.001$



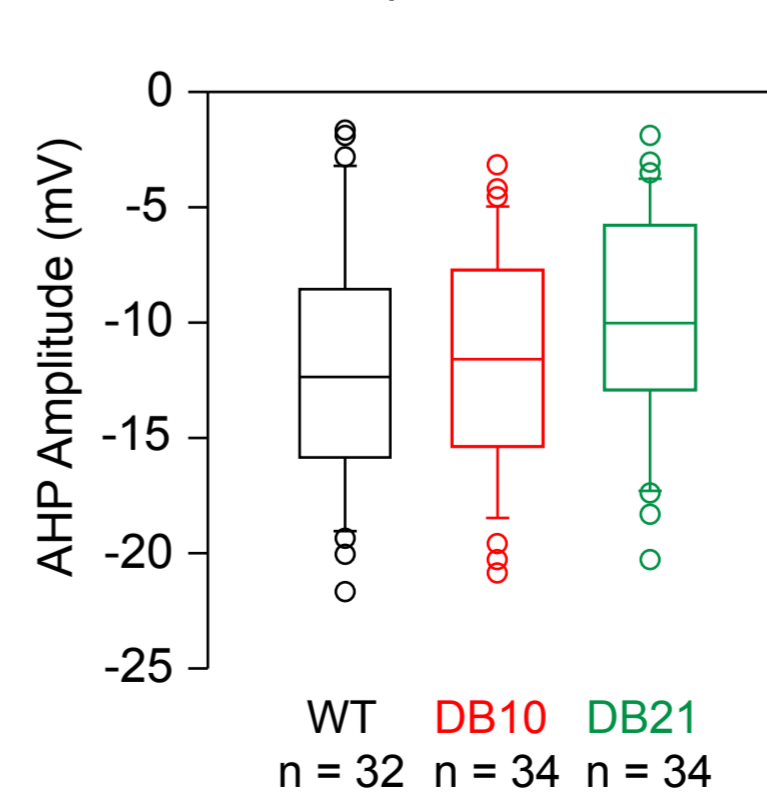
I AP Area, $p = 0.002$



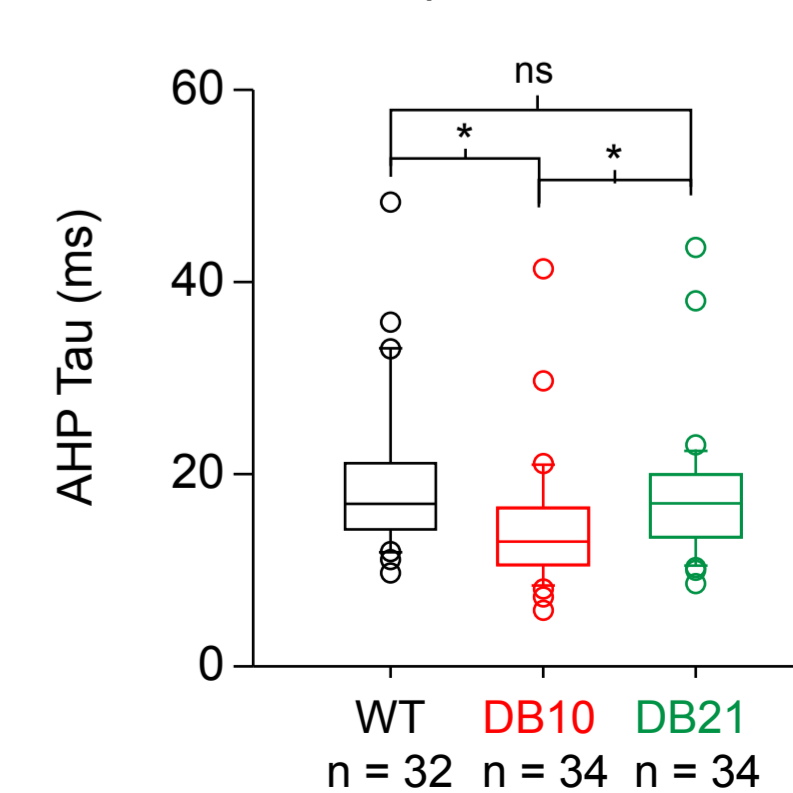
J AHP Area, $p = 0.767$



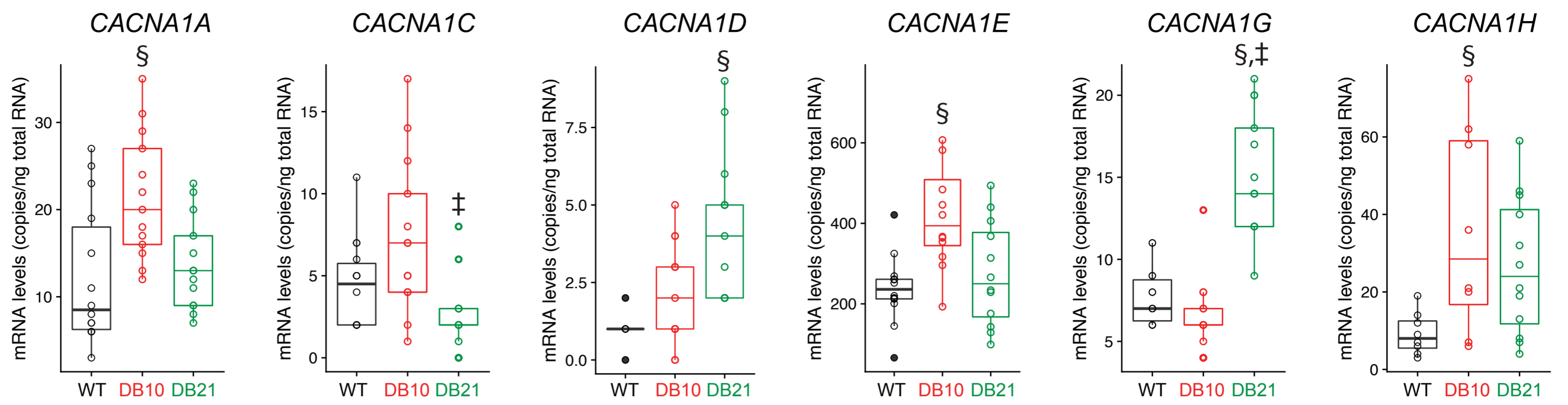
K AHP Amplitude, $p = 0.235$



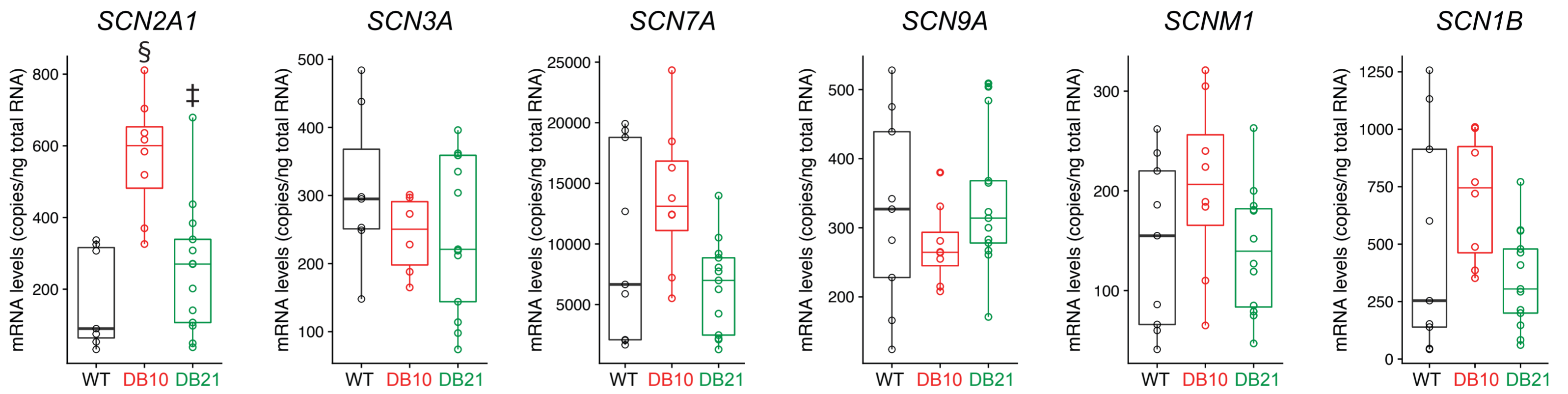
L AHP Tau, $p = 0.003$



Calcium Channels

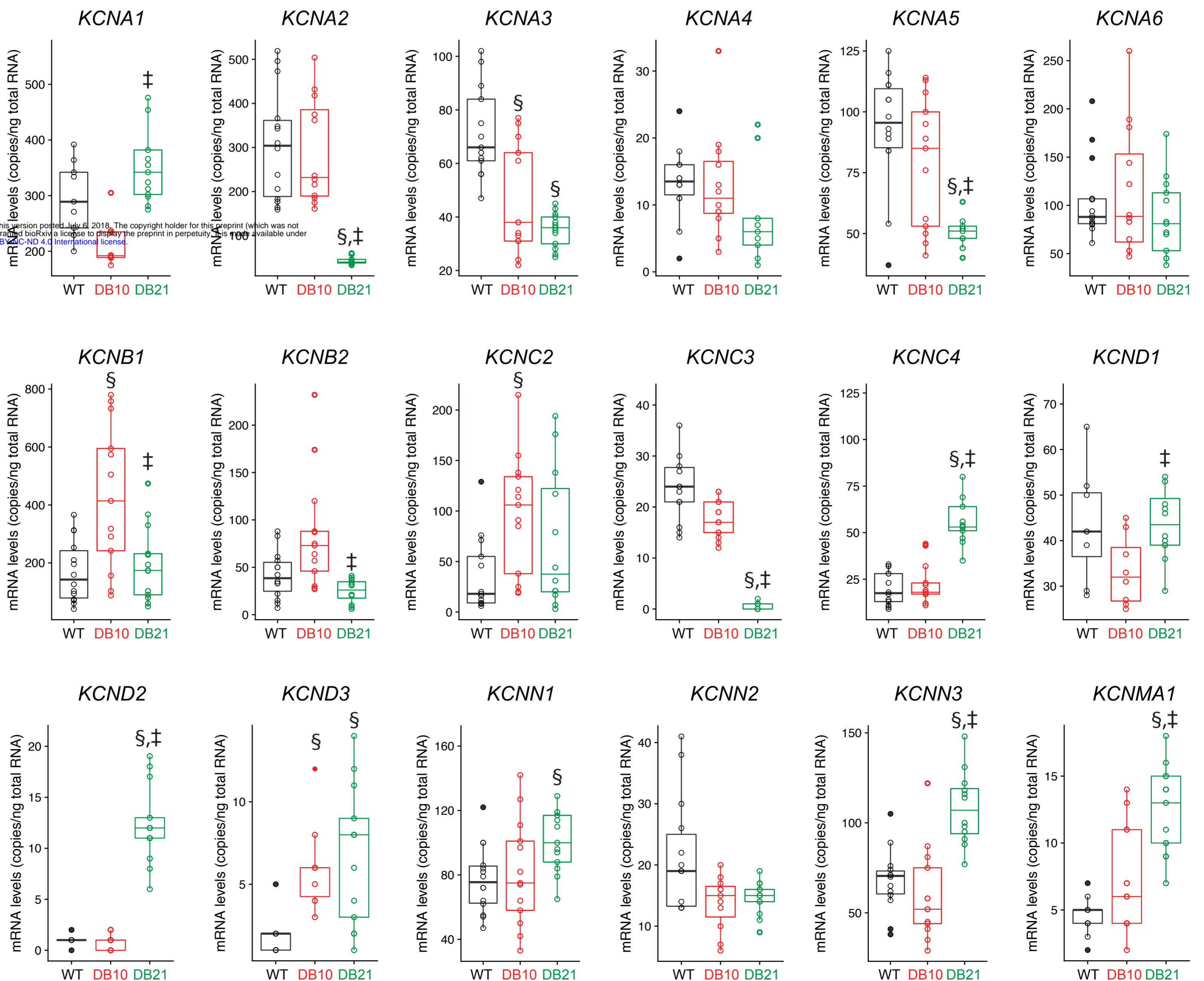


Sodium Channels



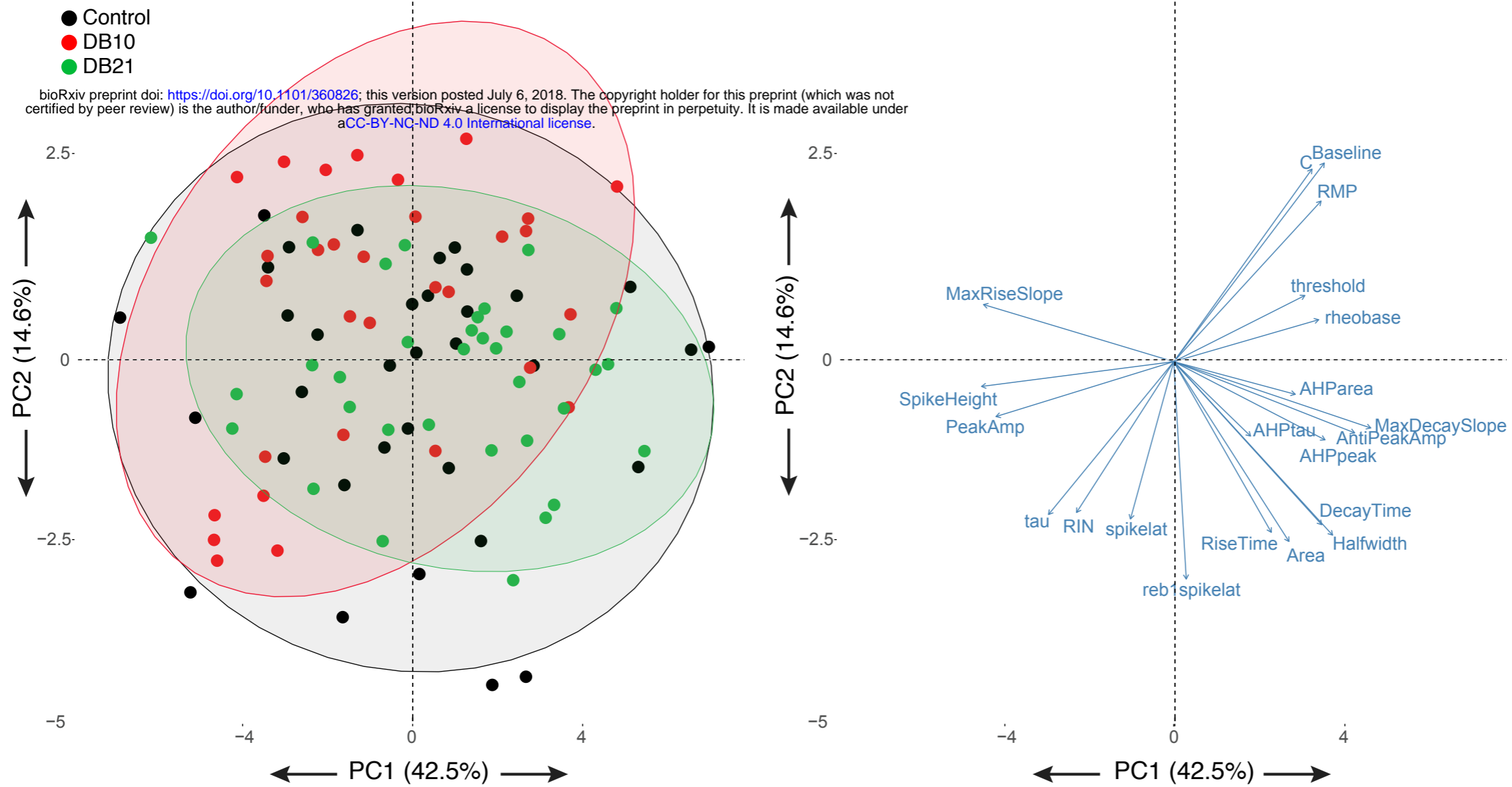
Potassium Channels

bioRxiv preprint doi: <https://doi.org/10.1101/360826>; this version posted July 6, 2018. The copyright holder for this preprint (which was not certified by peer review) is the author/funder, who has granted bioRxiv a license to display the preprint in perpetuity. It is made available under aCC-BY-NC-ND 4.0 International license.

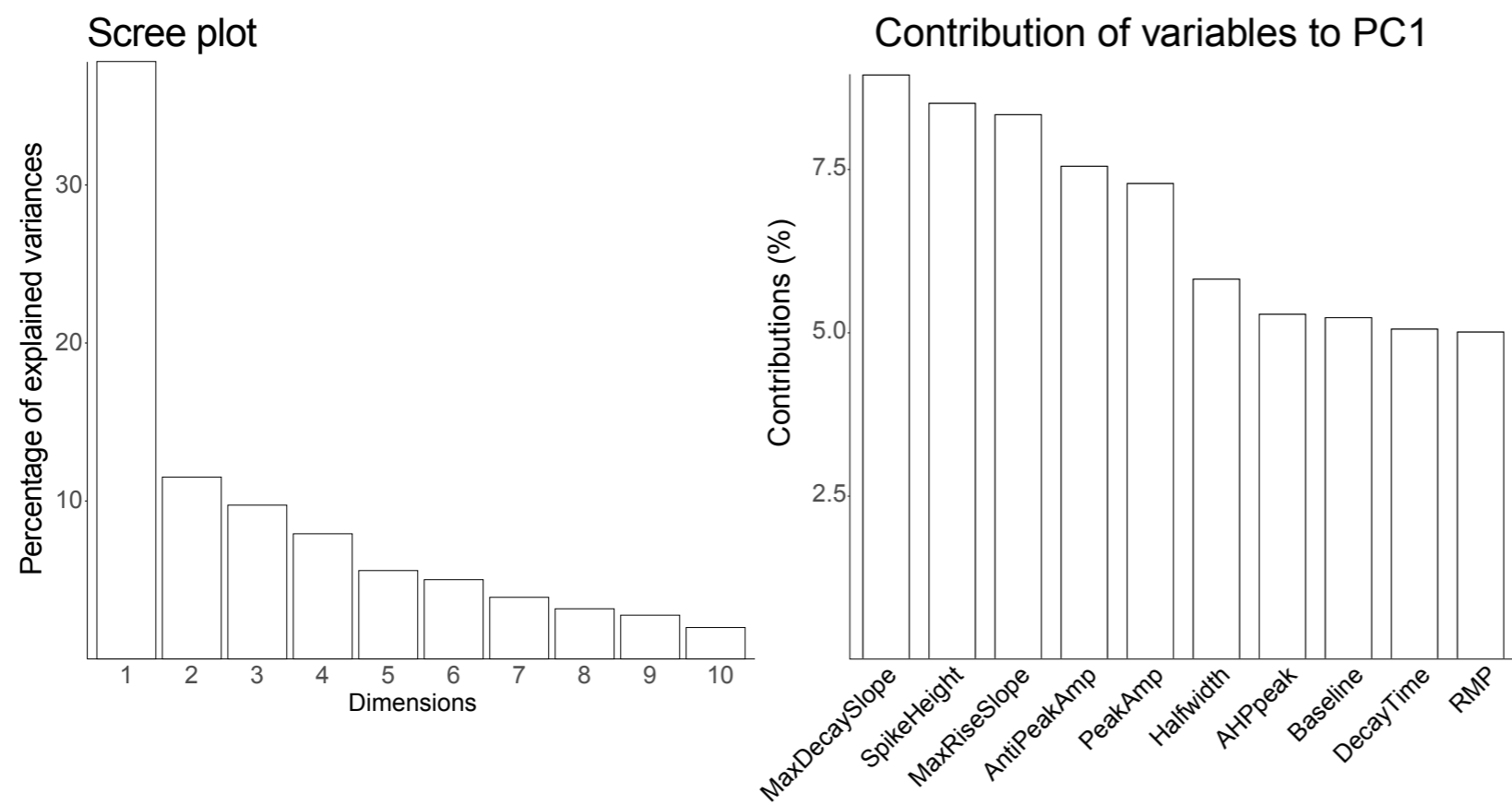


§ = diff from Control
‡ = DB10 diff from DB21

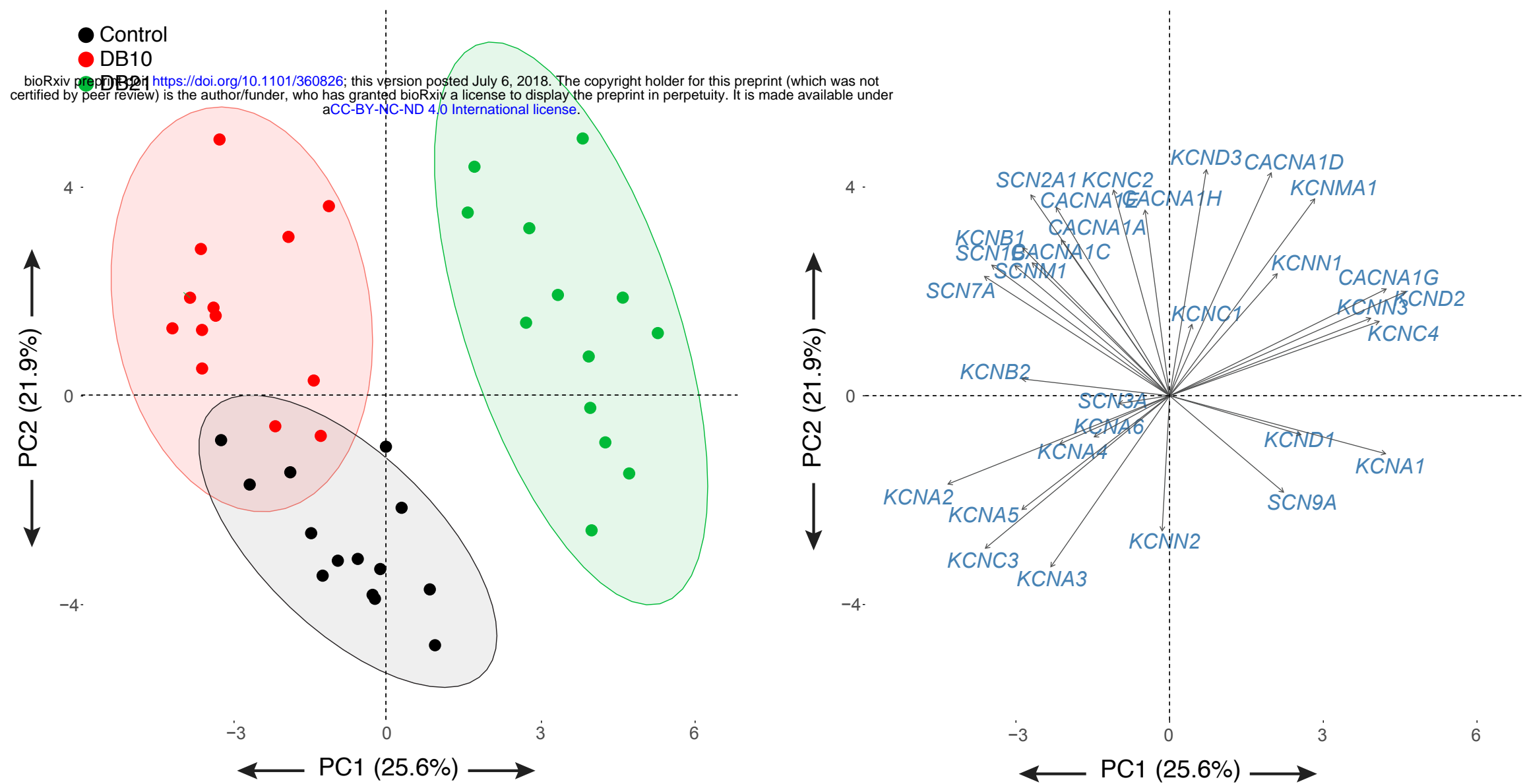
A.



B.



A.



B.

